Molecular Therapy
Oncology
Original Article

hsa-miR-5688 inhibits FOXC1-OCT4/SOX2 feedforward loop that drives chemoresistance in breast cancer stem cells

Apratim Dutta,[1,4] Sourio Chakraborty,[1,4] Apoorva Bhattacharya,[1] Udit Basak,[1] Subhadip Pati,[1] Sumon Mukherjee,[1] Deblina Guha,[1] Shruti Banerjee,[1] Nibedita Ray Chaudhuri,[2] Diptendra Sarkar,[3] Kuladip Jana,[2] Gaurisankar Sa,[1] Shubhra Ghosh Dastidar,[2] and Tanya Das[1]

[1]Centenary Building, Bose Institute, P-1/12, CIT Scheme VII M, Kolkata 700054, India; [2]Unified Academic Campus, Bose Institute, HCGJ+4X5, EN Block, Sector V, Bidhannagar, Kolkata, West Bengal 700091, India; [3]Department of Surgery, IPGMER and SSKM Hospital, Kolkata 700020, India

Inherently chemotherapy-resistant breast cancer stem cells (CSCs) are responsible for tumor initiation, metastasis, and relapse. CSCs "acquire" more resistance and stemness upon chemotherapy, thereby making relapse-free survival extremely challenging. Here, we describe a novel role of FOXC1 in "acquired resistance" of breast CSCs during chemotherapy. Putative binding sites of pluripotency factors OCT4 and SOX2, but not NANOG, on FOXC1 promoter, were demonstrated by JASPAR and validated by a docking experiment. Significant decline in FOXC1 expression was noticed after OCT4 or SOX2 ablation in breast CSCs. Contrastingly, presence of putative FOXC1 binding sites on the promoters of stemness genes and drug-resistance marker ABCG2, along with downregulation of OCT4 and SOX2 in FOXC1-ablated CSCs, indicated the existence of a feedforward FOXC1-OCT4/SOX2 transactivation loop in CSCs. Chemotherapy-induced upregulation of FOXC1, stemness, as well as drug resistance in CSCs, and downregulation of the same by prior FOXC1-ablation in *in-vitro* and *in-vivo* models, endorsed the contribution of this loop in chemo-induced acquisition of stemness and drug resistance. Finally, over-expression of hsa-miR-5688 sensitized CSCs toward chemotherapy and decelerated recurrence. Accordingly, we demonstrate a hitherto unknown mechanism underpinning chemotherapy-induced resistance in breast CSCs, causing relapse and identified hsa-miR-5688 as a potential therapeutic candidate for relapse-free survival of breast cancer patients.

INTRODUCTION

According to cancer stem cell (CSC) theory, breast CSCs, a subpopulation of self-renewing, chemo-resistant, tumor-initiating cells residing within the breast tumor[1,2] are largely accountable for drug-resistance, relapse, and poorer survival.[3,4] CSCs express the markers associated with stemness and pluripotency, such as OCT4, SOX2, NANOG, and ALDH1,[5] and elevated levels of several drug efflux pumps, such as MDR1, MRP1, and ABCG2,[6] and display an active DNA repair system, which aids in their drug-resistant phenotype, rendering them "non-targetable" by conventional therapeutic regimens.[7] Thus, although cancer patients initially respond well to chemotherapy, the development of chemo-resistance poses a major challenge in achieving relapse-free survival (RFS). Acquisition of chemo-resistance during treatment increases tumor-promoting characteristics, stemness,[8] and chemo-spared cells, which furnish enhanced expression of multi drug-resistance genes.[9–11] These CSCs remain dormant for years and cause recurrence after initial regression of the tumor upon neoadjuvant chemotherapy (NACT). It is, therefore, very important to unveil the mechanism underlying chemotherapy-induced acquisition of drug-resistance and stemness in cancer cells for developing new strategies to circumvent chemo-resistance, thus re-sensitizing breast CSCs toward chemotherapy and ensuring overall and RFS of the patients.

Recent research links the expression of FOXC1, a "fork-head box" (FOX) gene family member, which is a collection of extremely evolutionarily conserved genes[12] that share a 110 amino acid DNA-binding "FOX" domain, with poorer overall survival (OS) as well as lower brain metastasis-free survival in breast cancer.[13] Ectopic FOXC1 overexpression has been reported to induce more aggressive breast cancer characteristics, such as increased cell proliferation, migration, and invasion, along with epithelial-mesenchymal transition (EMT).[13] FOXC1 has been correlated to have a distinct connection with breast cancer clinical outcome in basal-like breast cancer (BLBC).[13] According to Wang et al.,[14] FOXC1 activates NF-κB signaling, which might be involved in FOXC1-induced BLBC proliferation, invasion, as well as migration.[14] FOXC1 has also been reported to be essential for the metastasis of hepatocellular carcinoma,[15] and the invasion-promoting role of FOXC1 might be dependent on higher expression of matrix metalloproteinase-7.[13,16] The

Received 28 September 2024; accepted 4 April 2025;
https://doi.org/10.1016/j.omton.2025.200982.

[4]These authors contributed equally

Correspondence: Prof. Tanya Das, ICMR Emeritus Scientist, Bose Institute, P-1/12, CIT Scheme VII M, Kolkata 700054, India.
E-mail: tanya@jcbose.ac.in

development and the occurrence of Hodgkin's lymphoma have both been reported to be linked to FOXC1 overexpression.[17,18] Increased expression of FOXC1 expression is thought to be a probable marker in acute myeloid leukemia for failure during induction chemotherapy along with cancer relapse, implying that FOXC1 expression has prognostic and diagnostic value in clinical management of this disease.[19] Furthermore, across numerous cancer types, elevated FOXC1 expression may predict clinical aspects, such as higher pathological grade, malignant clinical manifestations, and poor patient outcomes.[13,15,20]

Notch and Hedgehog are recognized to be important pathways in CSC regulation.[21] FOXC1 has been reported to activate Notch pathway in endothelial cells,[22] and it enhances smoothened-independent Hedgehog signaling in BLBC,[23] underlining its significance in CSC regulation. Another recent study on non-small cell lung cancer (NSCLC) has indicated that FOXC1 stimulates β-catenin signaling to promote CSC phenotype by direct transactivation of β-catenin gene, and FOXC1 ablation was able to render cisplatin and docetaxel sensitivity.[24] However, there is hardly any report demonstrating the role of FOXC1 in acquired chemo-resistance and increased stemness during chemotherapy in CSCs. This suggests that FOXC1 might play a crucial regulatory role in chemo-resistant CSCs, thus making FOXC1 a possible molecular target for anti-CSC-based treatments for chemotherapy-resistant malignancies.

Recent research has opened up new drug development opportunities, both in terms of employing RNAi for the discovery of novel targets and therapeutic agents.[25–29] Multiple reports have elucidated the role of FOXC1 in microRNA (miRNA)-dependent pathways.[30,31] The miRNAs constitute a type of noncoding RNAs, 22–23 nucleotides in length, which govern the expression of genes by imperfect complementarity with the 3′ untranslated region (3′UTR) of target gene mRNA that promotes translational inhibition or mRNA degradation.[25,32] miRNA dysregulation has been shown to play an instrumental role in several cellular processes in cancer, notably metastasis, invasion, migration, and EMT.[25,32,33] Numerous studies have also demonstrated that miRNAs are tumor-promoting or tumor-inhibiting factors.[25,32,34] Also, a multitude of miRNA therapeutics have reached clinical development for treating cancers.[26–29,35]

Here, we report that doxorubicin (Dox) treatment of breast CSCs leads to higher expression of FOXC1 that transactivates OCT4, SOX2, NANOG, and drug-resistance marker ABCG2. OCT4 and SOX2, in turn, transactivate FOXC1, thus constituting a reciprocal feedforward loop and finally resulting in acquired stemness and chemo-resistance—a major cause of relapse after chemotherapy. FOXC1-ablated CSCs are not only sensitized toward Dox but also furnish slower cancer recurrence after a three-cycle Dox therapy in comparison to control CSCs. Further explorations identified the candidature of hsa-miR-5688 in targeting FOXC1, thus essentially disrupting the feedforward loop and decreasing stemness and chemo-resistance in CSCs, thereby sensitizing these CSCs to Dox and delaying cancer-recurrence after three cycles of chemotherapy. This study is the first to report the role of FOXC1 in generating more aggressive breast CSCs during chemotherapy and provides a foundation for relapse-free breast cancer treatment by utilizing hsa-miR-5688.

RESULTS

Inherently chemo-resistant CSCs acquire more resistance during chemotherapy

When we treated breast cancer cell lines, MCF-7, MDA-MB-231, and MDA-MB-468, with 2.5-μM Dox for 24 h,[36–38] Dox induced significant apoptosis in non-stem cancer cell (NSCC) population (P3: $CD44^{-}/CD24^{-}$, $CD44^{-}/CD24^{+}$, $CD44^{+}/CD24^{+}$) but not in CSC population (P2: $CD44^{+}/CD24^{-}$) (Figure 1A). Next, breast CSC-enriched 2^0 spheres from MCF-7, MDA-MB-231, and MDA-MB-468 cells (Figure S1A), showing a higher percentage of CSCs (Figure S1B) and drug-resistance markers, i.e., ABCG2, MDR1, and MRP1 (Figure 1B), than corresponding cancer cells as evaluated by flow cytometry, confirmed that CSC-enriched 2^0 spheres are inherently more drug-resistant than corresponding cancer cells. Next, to understand whether chemotherapy aids in acquiring resistance in CSCs, we first sorted CSCs from all 2^0 spheres using MACS beads (Miltenyi Biotec) following manufacturer's protocol and verified that the expression levels of stemness factors *OCT4*, *SOX2*, *NANOG*, and *ALDH1* as well as drug-resistance markers *ABCG2*, *MDR1*, and *MRP1* were higher in CSCs as compared to their NSCC counterparts (Figures S2A–S2C). Subsequent experiments were performed using these CSCs. Treatment of these CSCs with 2.5-μM Dox for 24 h increased the expression of stemness and drug-resistance factors as determined by flow cytometry (Figure 1C), indicating Dox-induced gain in stemness and drug-resistance of CSCs and a possible contribution of such "acquired stemness and resistance" in tumor relapse post-chemotherapy. Our hypothesis has been supported by our previous report[38] depicting a close association between locoregional recurrence of disease with acquired resistance to therapy.

Chemotherapy increases FOXC1 expression along with lesser probability of overall and RFS

The previous results tempted us to explore the mechanism underlying acquisition of resistance by CSCs during chemotherapy. The role of FOXC1 in drug-resistance in NSCLC[24] and the influence of FOXC1 on the responsiveness of triple negative breast cancer to chemotherapy[23] have been reported recently. However, the role of FOXC1 in acquisition of resistance to chemotherapeutic by CSCs has not yet been well explored. Such lacuna of information tempted us to investigate the mechanism by which CSCs acquire resistance during chemotherapy in breast cancer. Our results depicted high expression of stemness and drug-resistance factors (Figure S2), and FOXC1, at both mRNA (Figure 2A) and protein (MFI) (Figure 2B) levels in breast cancer CSCs, in comparison to corresponding NSCCs. To further validate these results, CSCs and NSCCs from breast cancer patient tissues ($n = 5$) were MACS-sorted (CSCs: $CD44^{+}/CD24^{-}$; NSCCs: $CD44^{-}/CD24^{-}$, $CD44^{+}/CD24^{+}$, $CD44^{-}/CD24^{+}$) (patient details have been shown in Table S2). Our real-time qPCR data showed significantly higher ($p < 0.01$)

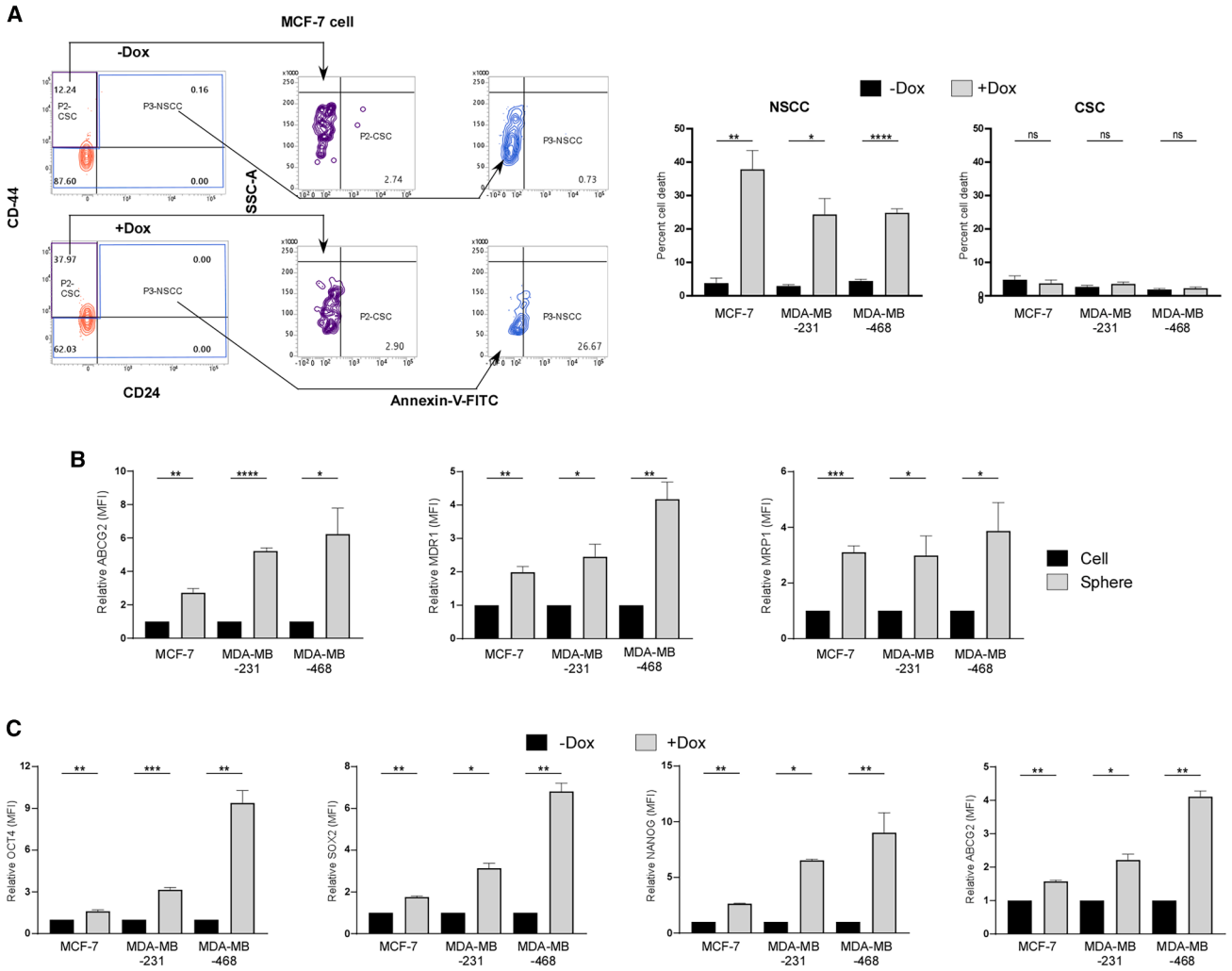

Figure 1. Inherently chemo-resistant CSCs acquire more resistance during chemotherapy

(A) Representative flow-cytometric plots depicting the gating strategy for $CD44^{+}/CD24^{-}$ CSC (P2) and $CD44^{+}/CD24^{+}$, $CD44^{-}/CD24^{-}$, $CD44^{-}CD24^{+}$ NSCC (P3) populations in MCF-7 cell (left panel). Bar diagrams depicting percentage of annexin-V-$FITC^{+}$ apoptotic cells in MCF-7/MDA-MB-231/MDA-MB-468 cell-derived gated NSCC and CSC populations in the presence of 2.5-μM Dox after 24 h of treatment (right panel). (B) Bar diagrams illustrating relative mean fluorescence intensity (MFI) of drug-resistance markers ABCG2 (left panel), MDR1 (middle panel), and MRP1 (right panel) in cells *vs.* respective 2^{0} spheres of MCF-7, MDA-MB-231, and MDA-MB-468, as analyzed by flow cytometry. (C) Bar diagrams showing relative MFI of stemness factors OCT4 (left panel), SOX2 (middle left panel), NANOG (middle right panel), and ABCG2 (right panel) as evaluated using flow cytometry in MCF-7, MDA-MB-231, and MDA-MB-468 CSCs in presence or absence of Dox, after 24 h of treatment. Data are mean ± SE or representative of three independent experiments unless otherwise noted. p = ns (non-significant), $^{*}p < 0.05$, $^{**}p < 0.01$, $^{***}p < 0.001$, and $^{****}p < 0.0001$ by unpaired Student's t test.

expression of *FOXC1* in patient-derived CSCs as compared to corresponding NSCCs (Figure 2C). Since FOXC1 expression in CSCs was in the order MDA-MB-468>MDA-MB-231>MCF-7, further studies were done using MDA-MB-468-derived CSCs. The flow cytometry results shown in Figure 2D, revealing an increase in FOXC1 expression upon Dox treatment, tempted us to explore the role of FOXC1, if any, in acquired resistance in breast cancer patients. To that end, first we analyzed *FOXC1* expression in patients with/without chemotherapy. Data obtained from publicly available GEO and R2: genomics analysis and visualization platform database[39] (GSE69031 and GSE28844) were divided into two cohorts, i.e., (1) chemo-naive and (2) chemotherapy-treated. In the GSE69031 dataset, breast cancer patients were treated with Dox and/or cytoxan (Figure 2E, left panel), whereas in the GSE28844 dataset, patients were treated with anthracycline and taxen-based NACT (Figure 2E, right panel) as the chemotherapy regimens. The results depicted significantly higher *FOXC1* expression in chemotherapy-treated patients as compared to chemo-naive ones in both the cases (Figure 2E). These data, therefore, indicated that not only FOXC1 expression is increased as a generic effect of chemotherapy treatment but also

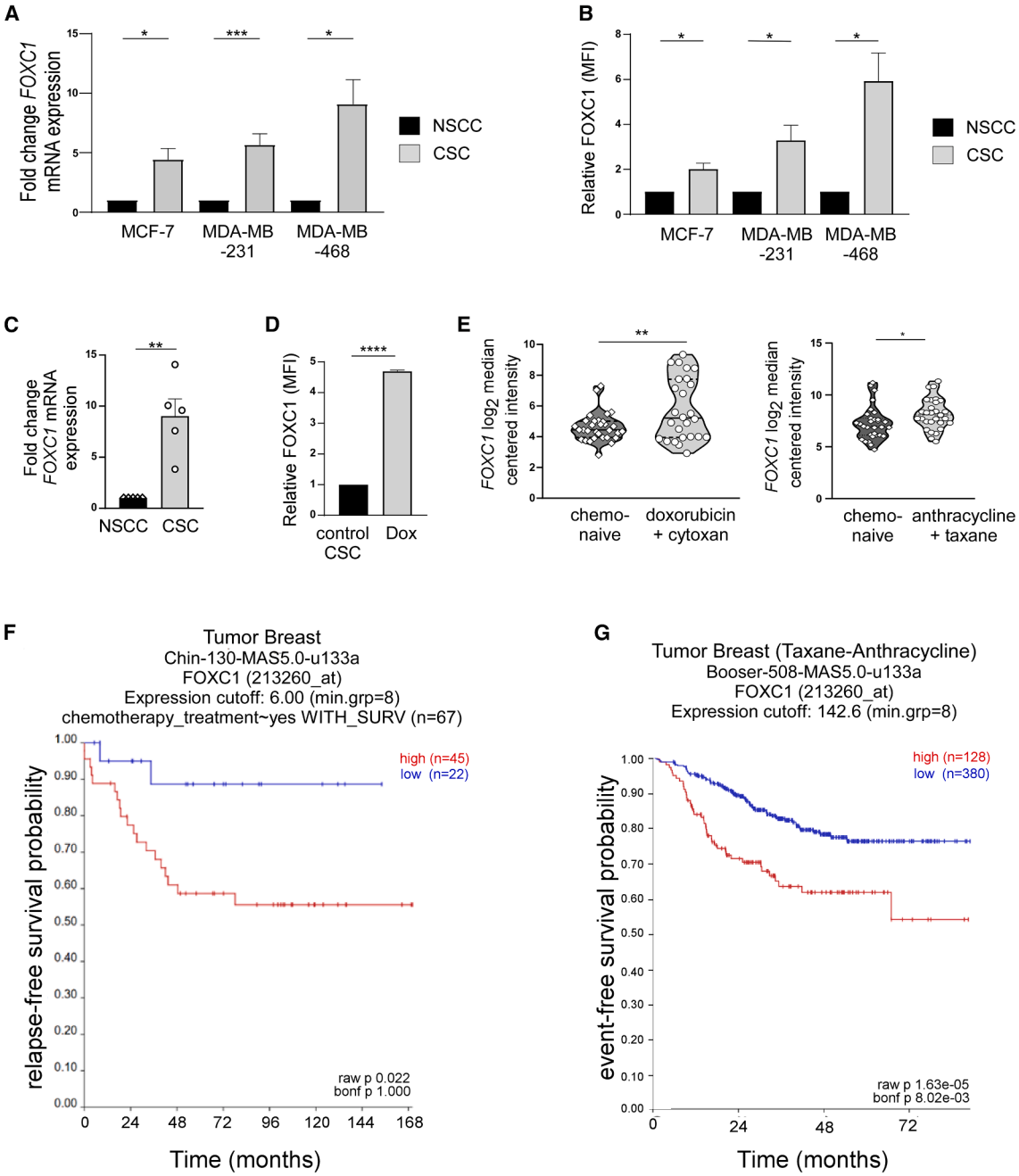

Figure 2. Chemotherapy increases FOXC1 expression along with lesser probability of overall and relapse-free survival

(A) Bar diagram depicting fold change of *FOXC1* mRNA expression in MACS sorted NSCC *vs.* CSC populations of MCF-7/MDA-MB-231/MDA-MB-468. (B) Bar diagrams portraying relative MFI of FOXC1 in MACS sorted NSCC *vs.* CSC populations of MCF-7/MDA-MB-231/MDA-MB-468 as determined by flow cytometry. (C) Bar diagram representing fold change of *FOXC1* mRNA expression in MACS sorted NSCC *vs.* CSC populations of breast cancer patients ($n = 5$). (D) Bar diagram depicting relative MFI of FOXC1 using flow cytometry in MDA-MB-468 CSCs in presence or absence of Dox. (E) Volcano plots depicting *FOXC1* expression in chemo-naive *vs.* chemotherapy-treated breast cancer patients using GSE69031 (left panel) and GSE28844 (right panel) datasets from R2: Genomics Analysis and Visualization software. (F) Kaplan-Meier plot depicting lower relapse-free survival (RFS) (using GSE69031 dataset) and (G) event-free survival (using GSE28844 dataset) of breast cancer patients with higher FOXC1 cohort compared to lower FOXC1 expressing patient group in chemo-treated conditions. Data in (A) to (D) are mean ± SE or representative of three independent experiments unless otherwise noted. $^{*}p < 0.05$, $^{**}p < 0.01$, $^{***}p < 0.001$, and $^{****}p < 0.0001$ by unpaired t test (A–E).

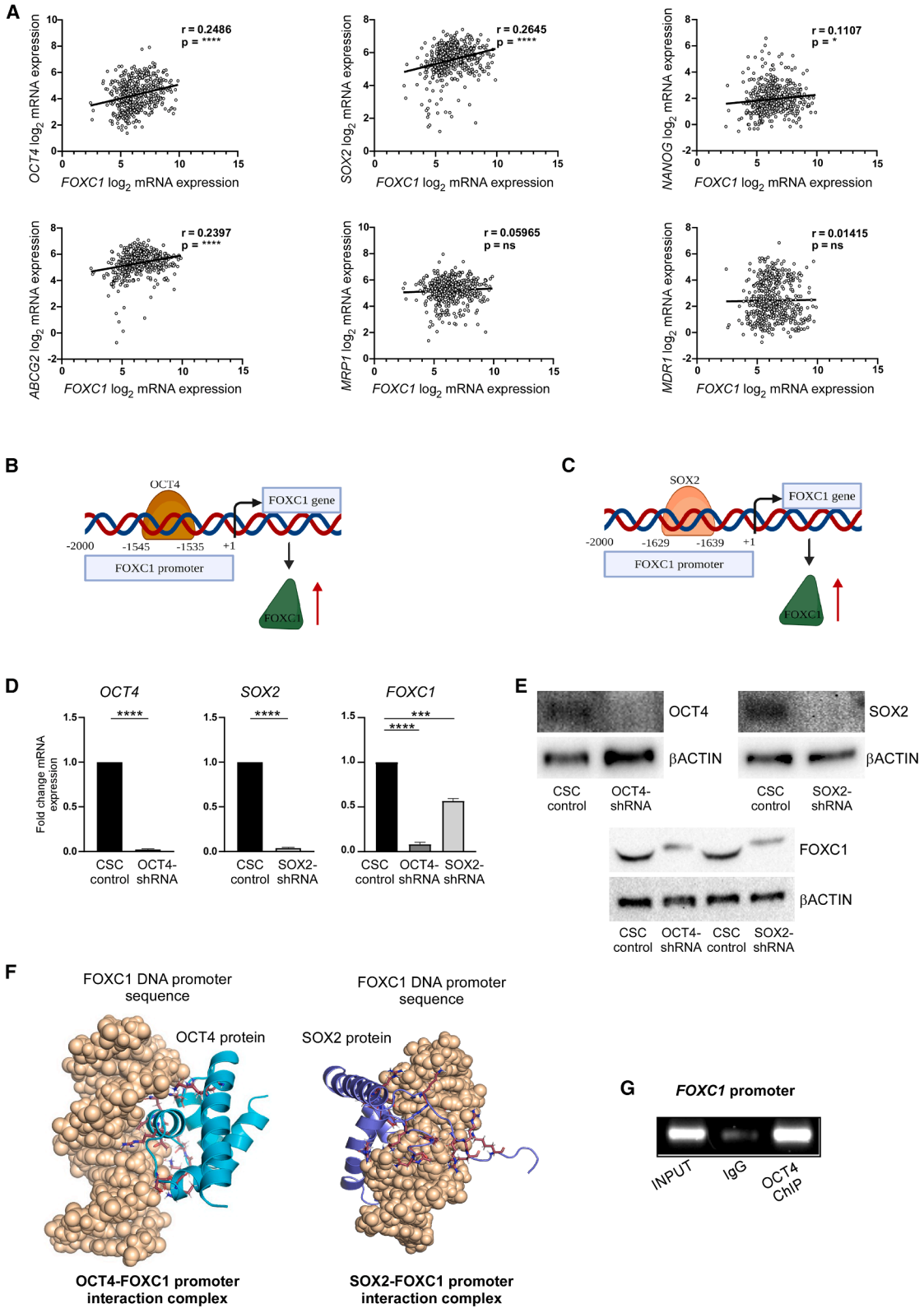

(legend on next page)

the possible relationship of *FOXC1* in gain-of-resistance in chemotherapy-treated breast cancer patients. To verify these results, we have used the endpoint data of GSE69031 and GSE28844 datasets, respectively, to predict survival probability of the breast cancer patients under study. Our *in-silico* analysis demonstrated that high *FOXC1* expression is significantly ($p < 0.05$) associated with a decreased probability of RFS of chemotherapy-treated breast cancer patients from GSE69031 dataset (Figure 2F). Again, high *FOXC1* expression was found to be significantly associated ($p < 0.0001$) with a decreased probability of event-free survival of chemotherapy-treated breast cancer patients from GSE28844 dataset (Figure 2G). Furthermore, breast cancer patients from Kaplan-Meier database[40] were divided into two groups, i.e., (1) chemo-naive and (2) NACT-treated, and their OS (Figure S3A) as well as RFS (Figure S3B) were analyzed. While there was no significant change in OS of different patients with higher or lower *FOXC1* expression from the chemo-naive group, NACT patients demonstrated significantly lower ($p < 0.05$) probability of OS with higher *FOXC1* expression compared to lower FOXC1-expressing patient cohort (Figure S3A). Similar results were also observed in the case of RFS of both groups (Figure S3B).

These results together indicate that FOXC1 expression, which was inherently higher in breast CSCs than in NSCCs, increased further in Dox-treated CSCs, indicating its probable role in regulating chemo-treated breast CSCs. Chemotherapy-induced increase in FOXC1 expression also raised the possibility of FOXC1 playing a significant role in acquisition of resistance upon chemotherapy exposure in breast cancer, thus declining OS and favoring relapse.

Identification of stemness factors as positive regulators of FOXC1 in CSCs

Considering our previous hypothesis, we next explored the correlation, if any, between expressions of FOXC1 and pluripotency, as well as drug-resistance factors among chemotherapy-treated breast cancer patients. To that end, first, we analyzed the *in-silico* breast cancer patient dataset from GEO and R2: genomics analysis and visualization platform database (GSE25066)[39] using *FOXC1* (Reporter ID: 213260_at), *OCT4* (Reporter ID: 208286_x_at), *SOX2* (Reporter ID: 214178_s_at), *NANOG* (Reporter ID: 220184_at), *ABCG2* (Reporter ID: 209735_at), *MRP1* (Reporter ID: 202805_s_at), and *MDR1* (Reporter ID: 209994_s_at). Interestingly, positive correlation was observed between *FOXC1 vs. OCT4* (R = 0.2486), *FOXC1 vs. SOX2* (R = 0.2645), and *FOXC1 vs. NANOG* (R = 0.1107), the three main stemness factors, as well as *FOXC1 vs. ABCG2* (R = 0.2397), the major breast cancer drug-resistance pump (Figure 3A) among breast cancer patients who were treated with aggressive chemotherapeutics as their first line of cancer treatment. However, no significant correlation was found between *FOXC1 vs. MRP1* (R = 0.060, p = ns) and *FOXC1 vs. MDR1* (R = 0.014, p = ns) (Figure 3A). Additionally, relevant *in-silico* analysis harnessing our previously investigated breast cancer patient dataset GSE69031, revealed significant (r = 0.3255, $p < 0.01$) association between *FOXC1* (Reporter ID: 213260_at) and *OCT4* (Reporter ID: 214532_x_at) among chemotherapy-treated breast cancer patients (Figure S4). Thereby, such findings further bolster the existing liaison between FOXC1 and OCT4 in breast cancer under chemotherapy-treated condition. Next, to check whether the (−2000 bp to +100 bp) long *FOXC1* promoter sequence, as obtained from the eukaryotic promoter database (EPD),[41,42] contains putative binding site(s) for OCT4, SOX2, and NANOG, we performed *in-silico* analysis using JASPAR database.[43] Results revealed putative OCT4 (−1535 bp to −1545 bp, binding score 10.5, relative score 0.9) (Figure 3B) and SOX2 (−1629 bp to −1639 bp, binding score 8.5, relative score 0.87) (Figure 3C) binding sites on the promoter of *FOXC1*. However, no putative binding site was observed for NANOG on *FOXC1* promoter. The shRNA-mediated ablation of *OCT4* or *SOX2* in MDA-MB-468 CSCs revealed a significant decline in the expression of FOXC1 at mRNA ($p < 0.0001$ for OCT4 and $p < 0.001$ for SOX2) (Figure 3D) as well as protein (Figure 3E) levels compared to the control sets for both the stemness factors, thus signifying the contributions of OCT4 and SOX2 in modulating FOXC1 expression in CSCs. Furthermore, our results indicated that the contributions of OCT4 toward regulating FOXC1 expression in CSCs are more than that of SOX2 (Figure S5A).

Next, validating the same, our *in-silico* docking demonstrated a distinct model of interaction between OCT4 and FOXC1 promoter sequence. Docking of OCT4 DNA-binding domain (DBD) with FOXC1 promoter sequence (Figure 3F, left panel) revealed a "ladder-like" binding pattern where the transcription factor holds the promoter stable by forming three stacked clusters of interface contacts along the major groove. The residues K154, R157, Q164 (top), K177, S180-T183, R186 (center), S193, K195, N196, and K199 (bottom) interact with sugar-phosphate backbone, whereas R186 directly interacts with the base of DNA. Similarly, our *in-silico* docking also furnished an interaction model between SOX2 and FOXC1 promoter sequence. The results revealed a nearly circular

Figure 3. Identification of OCT4 as a positive regulator of FOXC1 in CSCs

(A) Pearson correlation plots showing correlation between *FOXC1 vs. OCT4*, *FOXC1 vs. SOX2*, *FOXC1 vs. NANOG*, *FOXC1 vs. ABCG2*, *FOXC1 vs. MRP1*, and *FOXC1 vs. MDR1* from GSE25066 breast cancer patient dataset. (B) *In-silico* prediction of putative binding sites of OCT4 on *FOXC1* promoter and (C) SOX2 on *FOXC1* promoter, from JASPAR database. (D) Bar diagrams depicting fold change of *OCT4* mRNA expression in control *vs.* OCT4-shRNA-treated (left panel), *SOX2* mRNA expression in control *vs.* SOX2-shRNA-treated (middle panel), and *FOXC1* mRNA expression in control *vs.* OCT4-shRNA *vs.* SOX2-shRNA-treated (right panel) MDA-MB-468 CSCs. (E) Western blot images showing protein expression of OCT4, SOX2, and FOXC1 upon transient knock-down of OCT4 and SOX2 by treatment with their respective shRNA in MDA-MB-468 CSCs. βACTIN was used as internal loading control. (F) *In-silico* docking interaction of OCT4 on *FOXC1* promoter (left panel) and SOX2 on *FOXC1* promoter (right panel). (G) Representative semi-quantitative PCR data showing occupancy of OCT4 on *FOXC1* promoter in MDA-MB-468 CSCs using ChIP assay. Data in (D) is mean ± SE or representative of three independent experiments unless otherwise noted. p = ns, $^{*}p < 0.05$, $^{***}p < 0.01$, and $^{****}p < 0.0001$ by unpaired Student's t test (D).

DNA-binding pattern (Figure 3F, right panel) where the residues, such as N36, S37, R40-R43, N46, R53, R56, K65, N68, S69, K80, K109, and R113-K117, engage in direct polar interactions with the negatively charged DNA backbone, while R43, R98, and Y110 engage in direct interactions with the base of DNA. The docking scores have been listed in Table S3. Such favorable bindings of OCT4 and SOX2 on FOXC1 promoter lent further credence to the aforementioned findings, thus establishing that the transactivation regulation of FOXC1 is mediated by the stemness factors, OCT4 and SOX2. Finally, considering previous findings (Figures 3E and S5A), we took OCT4 as a model transcription factor and forward as well as reverse primers overlapping the potential binding regions were designed for *FOXC1* promoter, and binding of OCT4 on *FOXC1* target promoter region was confirmed by chromatin immunoprecipitation (ChIP) assay (Figure 3G).

These findings together substantiate the mechanisms underlying higher expression of FOXC1 in CSCs as compared to NSCCs.

FOXC1 transactivates stemness and drug-resistance factors in CSCs

Our subsequent investigation aimed at elucidating the contribution of FOXC1 on stemness gene expression. For the same, we first checked the expression levels of OCT4 and SOX2 in CSCs following shRNA-mediated ablation of *FOXC1*. Our results showed significant repression in the expression of OCT4 ($p < 0.0001$) and SOX2 ($p < 0.001$) at the mRNA levels (Figure 4A) as well as at the protein levels (Figures 4B and S5B) upon transient downregulation of FOXC1, hinting toward the existence of a reciprocal feedforward loop of FOXC1-OCT4/SOX2 in CSCs. To unravel the potential loop between FOXC1-OCT4/SOX2, we next aimed at identifying the probable DNA binding sites of FOXC1 on the (1) −2000 bp to +100 bp long promoter sequences of *OCT4* and *SOX2* as obtained from EPD.[41,42] To that end, first these promoter sequences were analyzed for presumed binding sites of FOXC1 by using JASPAR database.[43] In line with our hypothesis, putative FOXC1 binding sites were obtained on promoter regions of *OCT4* (−142 bp to −132 bp, binding score 10.7, relative score 0.91) (Figure 4C, upper panel) and *SOX2* (−726 bp to −716 bp, binding score 13.23, relative score 0.95) (Figure 4C, lower panel).

Subsequently, we performed *in-silico* docking experiments to visualize the binding of FOXC1 on these promoters. The structure of DBD among the FOX family of transcription factors, also known as the fork-head domain, is composed of three α-helices and two wing-like loops that allow these proteins to interact with DNA.[44] Our docking of FOXC1 DBD with all four promoter sequences revealed a common pattern of binding, the docking scores being listed in Table S4. Although the FOXC1 DBD inserts itself into the major groove of the DNA mainly *via* its α-helix 3, its overall structural fold also seems to play a significant role in stabilizing the complex state by adopting a "clipped" DNA-binding architecture. Several polar and positively charged residues at the interface, such as Y83, S125, R127, K138, K148, R169, R171, R172, and R173, were observed to singly form multiple hydrogen bonds with DNA backbone, thus clipping it uniformly along its length. The docking models thereby furnished the putative binding of FOXC1 on the promoters of *OCT4* (Figure 4D, left panel) and *SOX2* (Figure 4D, right panel), signifying a direct critical *in-silico* interaction between FOXC1 and OCT4/SOX2, further supporting our previous findings (Figures 4A and 4B). Next, to validate these *in-silico* results, forward and reverse primers overlapping the putative FOXC1 DNA-binding region were designed for the promoters of OCT4 and SOX2, and ChIP assay was performed. Our results validated the hitherto unreported binding of FOXC1 on the target promoter regions of *OCT4* and *SOX2* (Figure 4E).

Interestingly, *FOXC1*-ablation in MDA-MB-468 CSCs also reduced expression levels of *NANOG* and *ABCG2* (Figure 4F). *MRP1* and *MDR1* were not included in this experiment since no positive correlation was observed between FOXC1 *vs.* MRP1 and FOXC1 *vs.* MDR1 in our previous findings (Figure 3A). Next, using EPD[41,42] and JASPAR,[43] we further identified putative FOXC1 binding sites on the promoters of *NANOG* (−309 bp to −299 bp, binding score 8.9, relative score 0.90) (Figure 4G, upper panel) and *ABCG2* (−532 bp to −522 bp, binding score 12.6, relative score 0.94) (Figure 4G, lower panel). Further docking interaction showed predicted associations of FOXC1 on the promoters of *NANOG* (Figure 4H, left panel) and *ABCG2* (Figure 4H, right panel), with the docking scores being listed in Table S4. To verify the aforementioned *in-silico* data, we performed ChIP assay, which revealed a positive binding of FOXC1 on the promoters of *NANOG* and *ABCG2* in CSCs (Figure 4I), indicating the contribution of FOXC1 in overall generation of stemness and drug-resistance in CSCs.

These results, for the first time, provide a distinct model of interaction and binding of FOXC1 with the promoter sequences of pluripotency factors *OCT4*, *SOX2*, *NANOG*, and drug-resistance marker *ABCG2*.

Existence of a reciprocal feedforward transactivation loop between FOXC1 and pluripotency factors, OCT4 and SOX2, in CSCs that contribute in acquired resistance after chemotherapy

All the aforementioned furnished results together demonstrated the possibility of the existence of reciprocal transactivation loops between FOXC1 and pluripotency factors OCT4 and SOX2, in MDA-MB-468 CSCs. Validating our hypothesis, the ablation of OCT4 led to significantly reduced binding of OCT4 on *FOXC1* promoters, as observed using ChIP assay (Figure 5A, left panel) ($p < 0.001$), while the ablation of FOXC1 led to significantly lower binding of FOXC1 on *OCT4* (Figure 5A, right panel) ($p < 0.01$) and *SOX2* promoters (Figure 5B, left panel) ($p < 0.05$), explaining the previously observed decrease in *FOXC1* in *OCT4*-ablated CSCs as well as decrease in *OCT4* and *SOX2* expression levels in *FOXC1*-ablated ones (Figures 3D and 4A respectively). Similarly, reduced FOXC1 binding on *NANOG* (Figure 5B, middle panel) and *ABCG2* (Figure 5B, right panel) promoters in FOXC1-ablated CSCs were observed by ChIP assay. These collective results

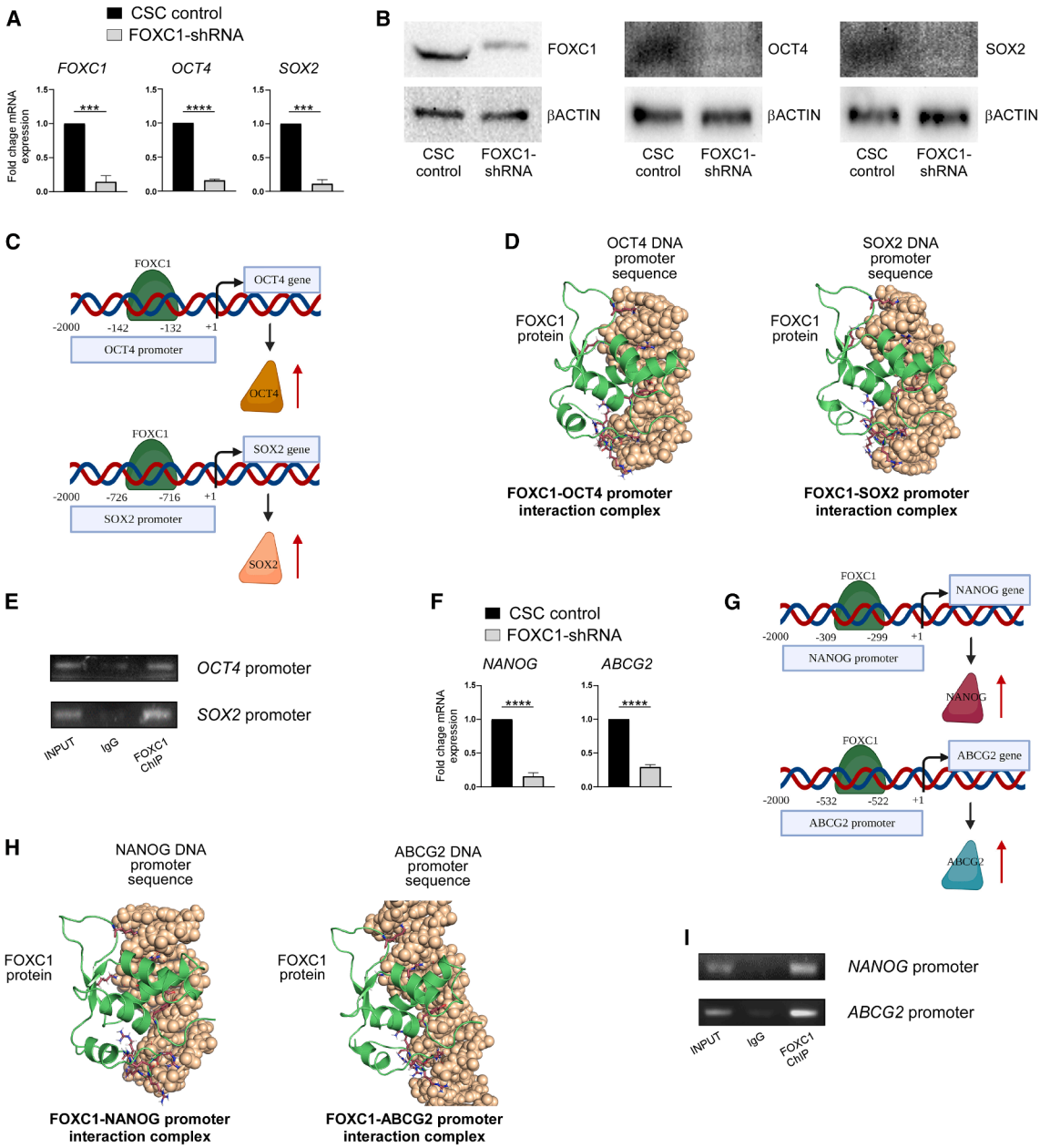

Figure 4. FOXC1 transactivates OCT4 and other stemness and drug-resistance factors in CSCs

(A) Bar diagrams depicting fold change in mRNA expression levels of *FOXC1*, *OCT4*, and *SOX2* in control *vs.* FOXC1-shRNA-treated MDA-MB-468 CSCs. (B) Western blot images showing protein expression of FOXC1 (left panel), OCT4 (middle panel), and SOX2 (right panel) upon transient knockdown of FOXC1 by shRNA in MDA-MB-468 CSCs. βACTIN was used as internal loading control. (C) *In-silico* prediction of putative binding sites of FOXC1 on *OCT4* and *SOX2* promoters from JASPAR database. (D) *In-silico* docking interaction of FOXC1 on *OCT4* and *SOX2* promoters. (E) Representative data showing occupancy of FOXC1 on the promoters of *OCT4* and *SOX2* in MDA-MB-468 CSCs using ChIP assay followed by semi-quantitative PCR. (F) Bar diagrams portraying fold changes in the mRNA expression levels of *NANOG*, and *ABCG2* in control *vs.* FOXC1-shRNA-treated MDA-MB-468 CSCs. (G) *In-silico* prediction of putative binding sites of FOXC1 on *NANOG* and *ABCG2* promoters from JASPAR database. (H) *In-silico* docking interactions of FOXC1 on *NANOG* and FOXC1 on *ABCG2* promoter sequences. (I) Representative data of FOXC1 occupancy on the promoters of *NANOG*, and *ABCG2* in MDA-MB-468 CSCs using ChIP assay followed by semi-quantitative PCR. Data in (A) and (F) are mean ± SE or representative of three independent experiments unless otherwise noted. ***$p < 0.001$ and ****$p < 0.0001$ by unpaired Student's t test (A) and (F).

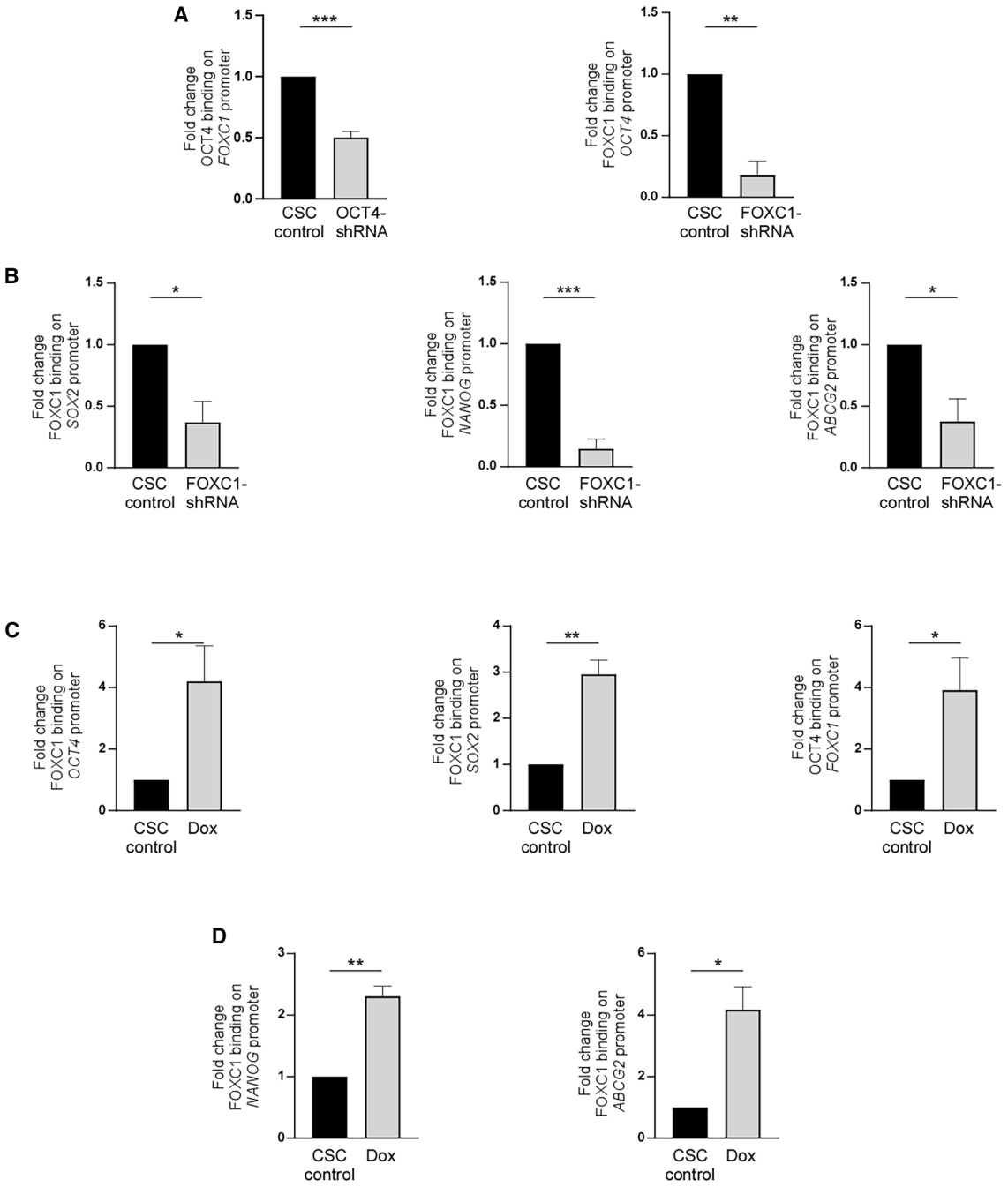

Figure 5. ChIP assay determines FOXC1-OCT4 reciprocal feedforward transactivation loop in CSCs

(A) Bar diagrams illustrating fold change in binding of OCT4 on *FOXC1* promoter (left panel) in control *vs.* OCT4-shRNA-treated and FOXC1 on *OCT4* promoter (right panel) in control *vs.* FOXC1-shRNA-treated MDA-MB-468 CSCs. (B) Bar diagrams portraying fold change in binding of: FOXC1 on *SOX2* (left panel), *NANOG* (middle panel), and FOXC1 on *ABCG2* (right panel) promoters in control *vs.* FOXC1-shRNA-treated MDA-MB-468 CSCs. (C) Bar diagrams depicting fold change of FOXC1-binding on *OCT4* promoter (left panel), FOXC1-binding on *SOX2* promoter (middle panel), and OCT4-binding on *FOXC1* promoter in control *vs.* Dox-treated MDA-MB-468 CSCs. (D) Bar diagrams showing difference in fold change of FOXC1-binding on *NANOG* (left panel) and *ABCG2* (right panel) promoters in control *vs.* Dox-treated MDA-MB-468 CSCs. Data are mean ± SE or representative of three independent experiments unless otherwise noted. *$p < 0.05$, **$p < 0.01$, and ***$p < 0.001$ by unpaired Student's t test.

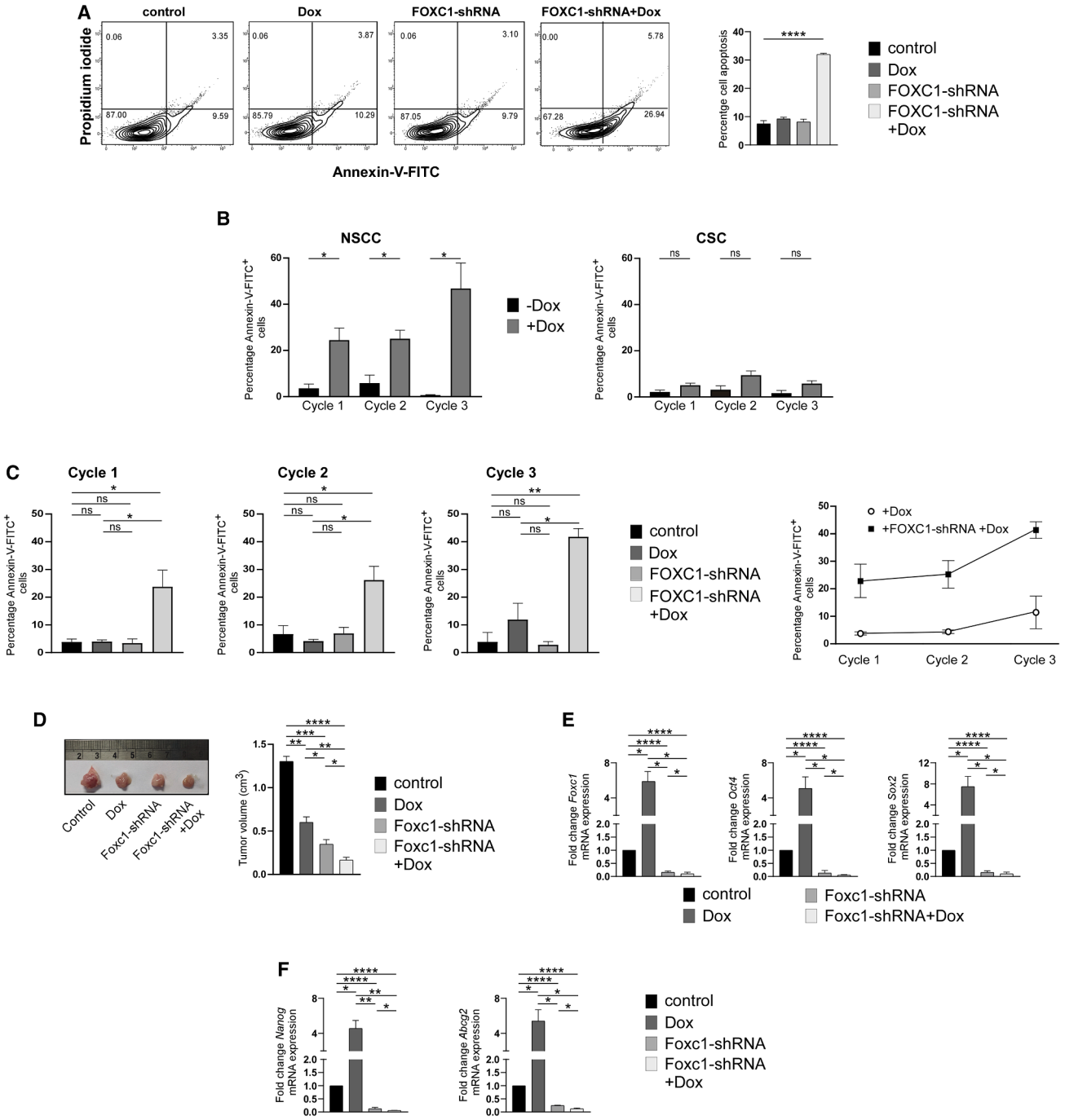

Figure 6. Downregulation of FOXC1 sensitizes CSCs toward chemotherapeutic drug doxorubicin

(A) Representative flow cytometry plots of annexin-V-FITC vs. propidium iodide (left panel), and bar diagram depicting percentage cell apoptosis (right panel) in MDA-MB-468 CSCs under the conditions: control, Dox-treated, FOXC1-shRNA-transfected, and FOXC1-shRNA-transfected + Dox-treated. (B) Bar diagrams depicting annexin-V-FITC$^+$ apoptotic cells following three cycles of Dox therapy in control *vs.* 3 cycles of Dox-treated NSCC (left panel) and CSC (right panel) subpopulations of MDA-MB-468 1^O spheres. (C) Bar diagrams showing percentage of annexin-V-FITC$^+$ apoptotic cells in MDA-MB-468 CSCs under the conditions of control *vs.* Dox *vs.* FOXC1-shRNA *vs.* FOXC1-shRNA + Dox during cycles 1–3 (left panel). Line plot portraying percentage of annexin-V-FITC$^+$ apoptotic cells for 1–3 cycles of Dox in control and FOXC1-shRNA-transfected MDA-MB-468 CSCs (right panel). The NSCC and CSC populations were selected after differential gating using FACS. (D) Representative image showing volumes

(legend continued on next page)

confirmed the existence of a reciprocal positive feedforward loop between FOXC1 and pluripotency factors, OCT4 and SOX2, but not with NANOG—since *in-silico* search did not reveal any putative binding site of NANOG on FOXC1 promoter sequence. However, this feedforward loop in turn upregulates NANOG and the drug-resistance marker ABCG2 in breast CSCs, thereby finally ensuring stemness and drug-resistance in these cells.

Finally, to validate the presence of aforementioned FOXC1-OCT4/SOX2 transactivation loop and its role in acquired resistance upon chemotherapy, CSCs were treated with Dox (2.5 μM), and ChIP assay was performed. Intriguingly, in Dox-treated CSCs, FOXC1-bindings to *OCT4* ($p < 0.05$) (Figure 5C, left panel) and *SOX2* ($p < 0.01$) (Figure 5C, middle panel) promoters were significantly increased. Finally, taking OCT4 as a model transcription factor, its binding to *FOXC1* promoter was also observed to be increased significantly ($p < 0.05$) as compared to control CSCs (Figure 5C, right panel). These results signified the critical role played by this positive feedforward transactivation loop toward higher expression levels of OCT4 (Figure 1C, left most panel), SOX2 (Figure 1C, left panel), and FOXC1 (Figure 2D) in Dox-treated CSCs. In line with our previous findings demonstrating Dox-induced upregulation of NANOG as well as ABCG2 (Figure 1C), we observed heightened FOXC1-binding on *NANOG* (Figure 5D, left panel) and *ABCG2* (Figure 5D, right panel) promoter regions upon Dox treatment.

All these findings from the ChIP assay followed by real-time qPCR analysis together confirm the existence of a reciprocal transactivation loop involving FOXC1, OCT4, and SOX2, which plays an important role in regulating the fate of CSCs itself and upon chemotherapy. In fact, chemotherapy-augmented FOXC1 further increased stemness and drug-resistance in CSCs, thus signifying chemo-mediated acquisition of stemness and drug-resistance by CSCs that might aid in breast cancer relapse.

Downregulation of FOXC1 sensitizes CSCs toward chemotherapeutic drug doxorubicin, even after multiple cycles

The aforementioned findings presenting FOXC1 as the master regulator of acquired resistance and stemness tempted us to explore the candidature of FOXC1 as a potential target to sensitize therapy-resistant CSCs. To that end, we analyzed cancer cell death perecentage upon Dox treatment (2.5 μM for 24 h) in control and FOXC1-ablated conditions. Dox failed to induce death in CSCs in controlled condition (Figure 6A), which might be due to inherent resistance of CSCs and their acquiring further resistance during chemotherapy. In FOXC1-ablated condition too, there was no significant change in apoptosis in CSCs (Figure 6A). These results signified that though FOXC1-ablation reduced stemness and chemo-resistance (Figures 4A and 4B), it failed to induce apoptosis in CSCs. Interestingly, though Dox alone failed to induce death in CSCs, it significantly induced apoptosis in FOXC1-ablated condition (Figure 6A). These results along with our already furnished data indicated that repression of FOXC1 expression not only inhibited inherent resistance and stemness, but also induced CSC apoptosis upon chemotherapy.

At this point, since cancer patients are given multiple cycles of chemotherapy, we examined whether FOXC1 can resist chemo-insult even after multiple cycles of chemotherapy. To that end, after three cycles of chemotherapy, as described in "materials and methods section," percent apoptosis in both NSCC and CSC subpopulations of MDA-MB-468 1^0 spheres were evaluated by flow cytometry, the gating strategy of which has already been furnished in Figure 1A. Results revealed increase in apoptosis of NSCCs with the increase in Dox cycle (Figure 6B, left panel). However, even after the third cycle, Dox failed to induce significant apoptosis in CSCs (Figure 6B, right panel), signifying high resistance of CSCs toward Dox. Interestingly, although FOXC1-ablation alone failed to induce significant apoptosis in FOXC1-ablated CSCs of MDA-MB-468 1^0 spheres, these transfectants underwent apoptosis upon Dox treatment (Figure 6C, left panel). Moreover, an increase in the number of treatment cycles increased percent apoptosis, resulting in ∼42% apoptosis after the third one (Figure 6C, left panel). A line plot portraying the percentage of apoptosis for Dox 1–3 cycles and FOXC1-shRNA-transfected + Dox has also been furnished (Figure 6C, right panel). These results demonstrated that neither Dox treatment nor FOXC1 ablation alone could induce CSC apoptosis. However, FOXC1 ablation sensitized CSCs toward Dox, thus resulting in significant CSC death after each chemotherapy cycle.

To re-validate our *in-vitro* results *in-vivo*, we next stably transduced scrambled shRNA (control) or Foxc1 lentiviral shRNA in 4T1 murine breast cancer cell line. The cells bearing Foxc1-shRNA were selected by puromycin selection from 1 μg/mL to 3 μg/mL over 2 weeks to obtain pure Foxc1-ablated 4T1 cells. The same number of both the control and Foxc1-ablated 4T1 cells were subjected to 2^0 sphere formation. The spheres although contained similar number of $CD44^+/CD24^-$ CSC populations (Figure S6A), Foxc1-ablated spheres showed decrease in expression of stemness and drug-resistance factors in comparison to the control spheres (Figure S6B). These results indicated that Foxc1-ablation, although downregulated the resistance and stemness potential of existing CSCs, did not significantly affect their numbers. Next, BALB/c mice were inoculated with these (1) control and (2) Foxc1-ablated 2^0 spheres. Each of these two sets of mice was further subdivided into (1) untreated and (2) Dox-treated sets. For Dox treatment, one week after tumor

of tumor generated in BALB/c mice (left panel), and bar diagrams depicting difference in their tumor volumes (right panel) in control *vs.* Dox *vs.* Foxc1-shRNA *vs.* Foxc1-shRNA+Dox-treated mice. (E) Bar diagram demonstrating fold change of *Foxc1* (left panel), *Oct4* (middle panel), and *Sox2* (right panel) mRNA expression in the tumor tissues of control *vs.* Dox *vs.* Foxc1-shRNA *vs.* Foxc1-shRNA+Dox-treated BALB/c mice. (F) Bar diagrams signifying fold change in mRNA expression levels of *Nanog* and *Abcg2* in tumors derived from control *vs.* Dox *vs.* Foxc1-shRNA *vs.* Foxc1-shRNA+Dox-treated BALB/c mice. Data are mean ± SE or representative of three independent experiments unless otherwise noted. $^*p < 0.05$, $^{**}p < 0.01$, $^{***}p < 0.001$, and $^{****}p < 0.0001$ by unpaired Student's t test.

formation, mice were injected intraperitoneally with 5 mg/kg Dox, every alternate day for 14 days after which the mice were sacrificed and eventually, final tumor volumes were measured. Our results presented highest tumor volume in control 4T1 2^0 sphere set, in comparison to all other three sets (Figure 6D). Dox-treated set furnished lower tumor volume than the control one (Figure 6D), which might be due to Dox-induced apoptosis of susceptible NSCCs (depicted in Figure 1A), which are the major population of cells of any tumor mass.[38] The tumor volume of Foxc1-ablated set was lower than both control and Dox-treated sets. Although Foxc1-ablation alone failed to furnish any significant alteration in breast CSC apoptosis in comparison to control CSCs (Figure 6A), such decrease in tumor volume of Foxc1-ablated set indicated lesser tumor progression due to reduced stemness (Figure S6B) and hence, lesser tumorigenicity of the CSCs present. Tumor volume of Foxc1-ablated + Dox-treated set was lowest as compared to all other 3 sets, indicating sensitization of otherwise resistant CSCs toward Dox due to ablation of Foxc1 (Figure 6D).

Furthermore, Dox-treated set furnished upregulated *Foxc1* (left panel), *Oct4* (middle panel), and *Sox2* (right panel) (Figure 6E) as well as the *Nanog* (Figure 6F, left panel) and *Abcg2* (Figure 6F, right panel), as compared to control, re-validating our previously obtained *in-vitro* data (Figures 1C and 2D). In contrast, there was a significant reduction in *Oct4* and *Sox2* (Figure 6E), *Nanog* as well as *Abcg2* (Figure 6F) in Foxc1-ablated set as Foxc1 ablation reduced downstream stemness and drug-resistance potential. Intriguingly, Foxc1-ablated + Dox-treated set depicted reduced expression of *Foxc1*, stemness factors, and drug-resistance marker, implying that unlike in only Dox-treated set, in Foxc1-ablated set, Dox could not rescue back the expressions of these factors.

In gist, our *in-vivo* results indicate that although Dox treatment led to smaller tumor formation than control due to possible targeting of the NSCC subpopulation inside the tumor, it increased the levels of *Foxc1*, *Oct4*, *Sox2*, *Nanog*, and *Abcg2* in the tumors of these mice. These findings re-validated the effect of Foxc1 in gain-in-stemness and drug-resistance and that ablation of Foxc1 can chemo-sensitize CSCs ultimately aiding in tumor regression in mice by doxorubicin.

FOXC1 ablation sensitizes CSCs toward chemotherapy by downregulating stemness and decreasing drug-resistance

Aforementioned results tempted us to understand the mechanism underlying apoptosis of FOXC1-ablated CSCs after the third cycle of chemotherapy, for which, after third chemotherapy cycle, the aforementioned four sets were MACS-sorted to obtain pure CSCs. Our results showed that the expression levels of FOXC1 (Figure 7A, left panel), OCT4 (Figure 7A, middle panel), and SOX2 (Figure 7A, right panel) were higher in Dox-treated CSCs as compared to control ones as determined using flow cytometry. In contrast, FOXC1-ablated CSCs furnished lower expressions of all these factors as compared to control. Interestingly, FOXC1-ablated + Dox-treated CSCs also depicted reduced expression of FOXC1 and all these markers of CSCs, again highlighting that Dox could not enhance their expression levels in FOXC1-ablated CSCs, even after third cycle. Furthermore, while Dox increased NANOG (Figure 7B, left panel) and ABCG2 (Figure 7B, right panel) expression after third cycle, FOXC1-ablated + Dox-treated CSCs depicted diminished expression of NANOG and ABCG2 as monitored by flow cytometry, implying Dox also could not salvage the expression of the stemness and drug-resistant factor up on FOXC1 downregulation. All these findings together elucidate the vital role of FOXC1 as the master regulator of CSC-associated stemness and drug resistance after tricycle chemotherapy and FOXC1-ablation causes downregulation of the aforementioned CSC factors, ultimately leading to sensitization of these "invincible CSCs," thus eventually resulting in CSC apoptosis by three-cycle Dox treatment.

Validating these results, when same numbers (1×10^4) of CSCs from the aforementioned four sets were subjected to sphere formation assay in serum-free medium (SFM) for a period of 7 days, Dox-treated CSCs furnished largest spheres in comparison to the spheres generated by other three sets, indicating that three cycles of Dox enhanced the CSC-properties, specifically the sphere forming ability (Figure 7C). In contrast, FOXC1-ablated set formed smaller spheres as compared to control CSCs, once again highlighting the efficacy of downregulated FOXC1 in impeding sphere forming ability of CSCs. Intriguingly, FOXC1-ablated + Dox-treated CSCs demonstrated the smallest spheres as compared to the other three sets, revealing the combinatorial effect in which downregulation of FOXC1 sensitized CSCs toward Dox, which in turn either underwent apoptosis or became further "weakened" and lost their properties.

Decrease in FOXC1 inhibits recurrence after chemotherapy

A multitude of reports signify the crucial role of CSCs in tumor recurrence after the initial "successful" chemotherapy.[3,4,38,45,46] Considering these reports as well as our previous results, we next explored the ability of the CSCs to form colonies after removal of Dox, in serum-containing media that supports CSC-differentiation and NSCC generation, thus mimicking tumor recurrence. To that end, same number (1×10^4) of MACS-sorted CSCs of the aforementioned sets were cultured in serum-containing differentiation media for 72 h. The results shown in Figure 7D demonstrated the formation of largest recurrent colonies by the Dox-treated CSCs as compared to all the other three sets, reflecting the higher recurrence potential of these aggravated CSCs after the removal of therapy. In contrast, FOXC1-ablated CSCs formed smaller recurrent colonies with respect to control, signifying that downregulated FOXC1 inhibited CSC characteristics, thereby hampering colony forming ability as well. Interestingly, FOXC1-ablated + Dox-treated CSCs formed smallest recurrent colonies with respect to all other aforementioned sets within this time, indicating FOXC1 ablation-induced impairment in the colony formation by CSCs got aggravated by Dox-induced additional stress that ultimately resulted in the formation of smallest recurrent colonies by those remaining CSCs that escaped Dox-induced apoptosis (Figure 7D). These results signified that while Dox alone significantly increased the ability of CSCs to

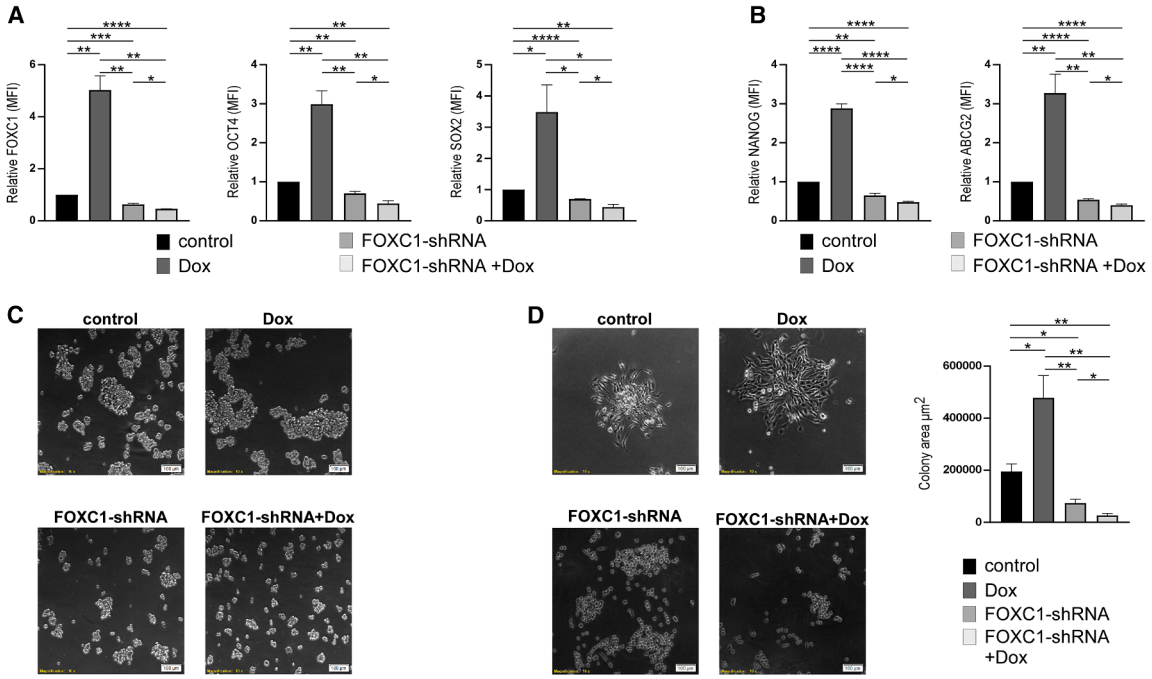

Figure 7. Downregulation of FOXC1 inhibits recurrence after chemotherapy

(A) Bar diagrams showing relative MFI of FOXC1 (left panel), OCT4 (middle panel), and SOX2 (right panel) in control *vs.* 3rd cycle of Dox *vs.* FOXC1-shRNA *vs.* FOXC1-shRNA + 3rd cycle of Dox-treated MDA-MB-468 CSCs, as determined by flow cytometry. (B) Bar diagrams showing relative MFI of NANOG (left panel) and ABCG2 (right panel) in control *vs.* 3rd cycle of Dox-treated *vs.* FOXC1-shRNA *vs.* FOXC1-shRNA + 3rd cycle of Dox-treated MDA-MB-468 CSCs, as evaluated by flow cytometry. (C) Phase contrast images of sphere formation assay of control *vs.* Dox *vs.* FOXC1-shRNA *vs.* FOXC1-shRNA + Dox-treated MDA-MB-468 CSCs after 3rd cycle of consecutive Dox treatment. (D) Phase contrast images showing recurrent colony formation of control *vs.* Dox *vs.* FOXC1-shRNA *vs.* FOXC1-shRNA+Dox-treated MDA-MB-468 CSCs after cycle 3 of Dox treatment subjected to serum-containing differentiation media (left panel). Bar diagram depicting area of recurrent colonies formed in μm^2 (right panel). Data in (A), (B), and (D) are mean ± SE or representative of three independent experiments unless otherwise noted. *$p < 0.05$, **$p < 0.01$, ***$p < 0.001$, and ****$p < 0.0001$ by unpaired Student's t test.

promote tumor recurrence, FOXC1-ablation alone hindered the basal recurrence ability of CSCs, while Dox-escaped FOXC1-ablated transfectants furnished lowest tumor recurrence potential.

In a nutshell, our results revealed that even three cycles of Dox not only failed to induce CSC apoptosis, but also upregulated FOXC1-mediated gain-in-expression of stemness and drug-resistance markers, thereby ensuring survival of CSCs and aiding in formation of largest spheres, and differentiating to form largest colonies when kept in serum-containing media after the removal of therapy. These results together indicate enhancement of CSC-properties and possibilities of higher recurrence of tumor in patients. Conversely, although FOXC1-ablation itself did not induce any significant apoptosis in CSCs, it generated smaller spheres and differentiated colonies, highlighting the effect of FOXC1-ablation in hindering CSC-properties and their ability toward tumor-recurrence. Importantly, ablation of FOXC1 followed by three cycles of Dox not only induced significant CSC apoptosis but also repressed FOXC1-directed gain-in-stemness and gain-in-drug-resistance potential of Dox-escaped CSCs, if any. Moreover, in these FOXC1-ablated CSCs, three cycles of Dox significantly hindered both sphere propagation and differentiated recurrent colony formation, thus ultimately ensuring CSC apoptosis in one hand, while inhibiting CSC-characteristics in the escaped ones and thus breast cancer-recurrence after chemotherapy on the other.

Identification of novel miRNA to target FOXC1 expression as a tool to sensitize chemo-resistant CSCs

All the previous results implied the candidature of FOXC1 as a "target" for attenuating therapy-resistant CSCs. To that end, we first aimed at identifying a potential inhibitor of FOXC1 in CSCs. Since miRNAs block the translation of target proteins or directly degrade target mRNAs,[25,27] we next searched in both miRCarta[47] and Diana Tools micro-RNA database[48] using MicroT-CDS (cut-off value of $\geq$0.95) and obtained 24 miRNAs that can putatively target FOXC1 (Table S5). Among these, there was hardly any report demonstrating the presence and/or role of the 7 miRNAs in cancer, especially in CSCs. A recent study has reported that the expression of one of these 7 miRNAs, i.e., miRNA hsa-miR-5688, is high in normal tissue as compared to non-small cell lung carcinoma, while its overexpression downregulates IL-11 and inhibits tumor progression.[49] This information along with its high miTG score (0.969; Table S5) signified high probability of this miRNA targeting FOXC1 in breast CSCs. We, therefore, next explored the correlation of hsa-miR-5688 with

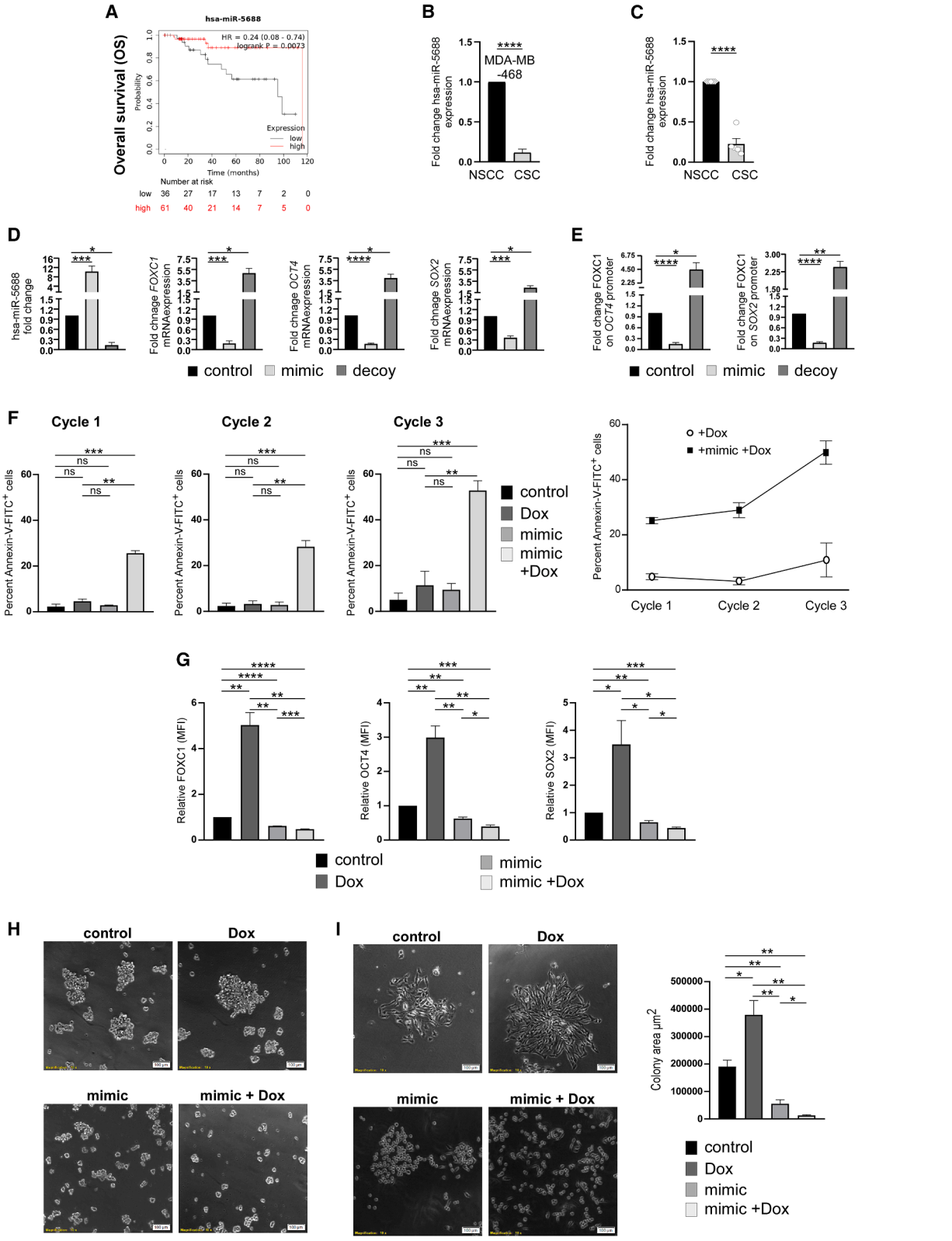

(legend on next page)

OS in breast cancer. Analysis of survival plots of hsa-miR-5688 from KM plotter database[40] revealed a positive correlation between hsa-miR-5688 expression and OS in triple negative breast cancer patients (Figure 8A).

Further experiments revealed a significantly reduced ($p < 0.0001$) expression of hsa-miR-5688 in MDA-MB-468-derived CSCs (Figure 8B), thus pointing toward an ingenious strategy of CSCs for ensuring their own survival. In line with these findings, hsa-miR-5688 expression was also significantly lower in the patient tumor tissue-derived CSCs as compared to the corresponding NSCCs (Figure 8C). At this juncture, our literature search revealed that human hsa-miR-5688 gene is encoded by chromosome-3 (85385710–85385792), the full-length hsa-miR-5688 gene being ~83 nucleotides long. The mature miRNA sequence of hsa-miR-5688 is *5′ UAACAAACACCUGUAAAACAGC 3′*, in which the *5′ AACAAA 3′* is the seed region which showed 100% complementarity with FOXC1 3′ UTR target site *5′ TTTGTT 3′*. These findings together further supported our view of utilizing hsa-miR-5688 for targeting *FOXC1*. For the same, MACS-sorted MDA-MB-468 CSCs were transfected with either sense hsa-miR-5688 (mimic) or anti-sense hsa-miR-5688 (decoy) and changes in expression of *FOXC1* were observed (Figure 8D). While mimic significantly ($p < 0.001$) repressed FOXC1 expression, decoy ($p < 0.05$) increased the same, thereby confirming the direct role of hsa-miR-5688 in FOXC1 regulation. Attenuating FOXC1 expression by hsa-miR-5688 mimic significantly decreased *OCT4* ($p < 0.0001$) and *SOX2* ($p < 0.001$) levels, while decoy significantly upregulated those ($p < 0.05$ for *OCT4* and $p < 0.05$ for *SOX2*) (Figure 8D), indicating the role of this miRNA in inhibiting the FOXC1-OCT4/SOX2 feedforward loop. The mimic also significantly downregulated *NANOG* ($p < 0.001$) (left panel) and *ABCG2* ($p < 0.0001$) (right panel) expression levels while decoy enhanced the same ($p < 0.05$ for *NANOG* and $p < 0.05$ for *ABCG2*) (Figure S7A).

These findings strengthened our hypothesis that overexpression of hsa-miR-5688 might inhibit FOXC1-OCT4/SOX2 feedforward loop thereby decreasing overall stemness and drug-resistance factors. Validating our conjecture, ChIP assay using mimic-transfected CSCs showed significantly reduced binding of FOXC1 on the promoters of *OCT4* ($p < 0.0001$) (left panel) and *SOX2* ($p < 0.0001$) (right panel) (Figure 8E), which might be due to the reduced expression of FOXC1 in comparison to un-transfected ones (Figure 8D). In contrast, higher FOXC1-binding was observed on *OCT4* ($p < 0.05$) (left panel) and *SOX2* ($p < 0.01$) (right panel) promoters in decoy-transfected CSCs (Figure 8E) validating their higher expression levels as shown in Figure 8D. A similar trend was also observed when transfection of mimic led to reduced FOXC1 binding on *NANOG* ($p < 0.001$) (left panel) and *ABCG2* ($p < 0.01$) (right panel) promoters (Figure S7B), which might be due to the lower expression of FOXC1 in comparison to control set (Figure 8D). Conversely, decoy transfection augmented the binding of FOXC1 to *NANOG* ($p < 0.001$) (left panel) and *ABCG2* ($p < 0.05$) (right panel) (Figure S7B), attributable to the increased expression of FOXC1 in decoy-transfected groups, as previously noted (Figure 8D). These results once again highlight the crucial role of FOXC1 in regulating stemness and drug-resistance factors, and that hsa-miR-5688 hampers acquisition of CSC-related stemness and drug-resistance by directly inhibiting *FOXC1* and indirectly, by inhibiting FOXC1-OCT4/SOX2 loop that further downregulates the expression of FOXC1-controlled downstream genes.

These findings supported our hypothesis that hsa-miR-5688 might act as a potent miRNA for breast CSC-sensitizing therapy by targeting *FOXC1* and thereby hindering FOXC1-mediated acquisition of stemness and drug resistance.

Targeting *FOXC1* by hsa-miR-5688 inhibits tumor recurrence

With the aim of exploring whether hsa-miR-5688 plays any role in inhibiting breast cancer-recurrence, MDA-MB-468 1^0 spheres were divided in four sets, (1) control, (2) Dox-treated, (3) hsa-miR-5688 (mimic)-transfected, and (4) mimic+Dox-treated. For this experiment, three cycles of Dox were administered as mentioned previously. Utilizing flow cytometry and gating the CSC sub-population as shown previously (Figure 1A), after each cycle, we assessed CSC apoptosis in these sets. Our results demonstrated significant ($p < 0.01$) apoptosis after each of the three cycles in the mimic + Dox-treated set only (Figure 8F, left panel). Furthermore, the percent apoptosis increased in this set with the increase in number of therapy cycles, with (~46%) apoptosis after the third one (Figure 8F, left panel). These findings demonstrated that neither Dox nor mimic triggers CSC apoptosis when applied alone, but prior upregulation

Figure 8. Identification of novel miRNA targeting FOXC1 expression for sensitizing chemo-resistant CSCs

(A) KM plot of triple negative breast cancer patients correlating higher probability of OS with higher expression of hsa-miR-5688. (B) Bar graphs illustrating the difference in expression levels of hsa-miR-5688 between MACS-sorted MDA-MB-468 NSCCs and CSCs and (C) breast cancer patient-derived NSCCs *vs.* CSCs ($n = 5$). (D) Bar diagrams portraying fold change in expression levels of hsa-miR-5688, *FOXC1*, *OCT4*, and *SOX2* in control *vs.* mimic-treated *vs.* decoy-treated MDA-MB-468 CSCs. (E) Bar diagrams depicting difference in fold change of FOXC1-binding on *OCT4* and *SOX2* promoters in control *vs.* mimic-treated *vs.* decoy-treated MDA-MB-468 CSCs. (F) Bar diagrams showing percentage of annexin-V-FITC$^+$ apoptotic cells in control *vs.* 1–3 cycles of Dox-treated *vs*. mimic *vs.* mimic + 1–3 cycles of Dox-treated MDA-MB-468 CSCs (left panel). Line plot indicating the same in 1–3 cycles of Dox-treated *vs*. mimic *vs.* mimic + 1–3 cycles of Dox-treated MDA-MB-468 CSCs (right panel). (G) Bar diagrams showing relative MFI of FOXC1 (left panel), OCT4 (middle panel) and SOX2 (right panel) in control *vs.* 3rd cycle Dox-treated *vs.* mimic *vs.* mimic + 3rd cycle Dox-treated MDA-MB-468 CSCs, as validated using flow cytometry. (H) Phase contrast images of sphere formation assay of control *vs.* 3rd cycle Dox-treated *vs.* mimic *vs.* mimic + 3rd cycle Dox-treated MDA-MB-468 CSCs. (I) Phase contrast images of recurrent colony formation assay in control *vs.* 3rd cycle Dox-treated *vs.* mimic *vs.* mimic + 3rd cycle Dox-treated MDA-MB-468 CSCs when exposed to serum-containing differentiation media (left panel). Bar diagram depicting area of recurrent colonies formed per μm^2 (right panel). Data in (B) to (G), and (I) are mean ± SE or representative of three independent experiments unless otherwise noted. p = ns, $^*p < 0.05$, $^{**}p < 0.01$, $^{***}p < 0.001$, and $^{****}p < 0.0001$ by unpaired Student's t test (B) to (G), and (I).

of hsa-miR-5688 sensitizes CSCs to Dox, with considerable CSC-mortality after each cycle. A line plot for each of the three Dox cycles has been furnished to demonstrate in detail the percent CSC apoptosis of Dox-treated *vs.* mimic + Dox sets (Figure 8F, right panel).

After the third cycle of Dox, aforementioned four sets were MACS-sorted to obtain pure CSCs. Our flow cytometry results revealed that FOXC1 (Figure 8G, left panel), OCT4 (Figure 8G, middle panel), and SOX2 (Figure 8G, right panel) expression levels were higher in Dox-treated CSCs as compared to control CSCs, whereas those were lower in the mimic-transfected CSCs (Figure 8D). Additionally, following a similar pattern with the aforementioned results, expressions of NANOG ($p < 0.0001$) (Figure S8A, left panel) and ABCG2 ($p < 0.01$) (Figure S8A, right panel) were higher in Dox-treated CSCs as compared to control CSCs, while they were reduced in mimic-transfected CSCs (Figure S8A). Mimic + Dox-treated CSCs also depicted repressed levels of NANOG ($p < 0.01$) (Figure S8A, left panel) and ABCG2 ($p < 0.0001$) (Figure S8A, right panel). All these results implied that presence of upregulated hsa-miR-5688 hampered the efficacy of Dox-induced enhancement of these factors.

The aforementioned results indicate that heightening of hsa-miR-5688 impedes FOXC1 and consequently, OCT4 expression, which further hinders the reciprocal feedforward loop of FOXC1-OCT4. Direct curbing of FOXC1 expression by hsa-miR-5688 or by indirect disruption by FOXC1-OCT4 loop resulted in an attenuated expression of OCT4, other stemness, and drug-resistance genes, allowing Dox to destroy these CSCs as observed (Figure 8F). This demonstrates the significance of hsa-miR-5688 in regulating *FOXC1* and, in turn, FOXC1-OCT4 loop in directing the expression of stemness and drug-resistance genes. As a result, these CSCs become more sensitive to Dox, leading to CSC apoptosis (Figure 8F).

Next to determine if there was any alteration in the inherent sphere-forming property of CSCs, in the CSC sub-populations of the aforementioned sets, identical numbers of isolated CSCs (1×10^4) from those four sets were subjected to sphere formation assay in SFM for 7 days. We noted that Dox-treated CSCs developed largest spheres as compared to all the other sets (Figure 8H) demonstrating an aggravation in sphere-forming potential of CSCs post three cycles of Dox treatment. Furthermore, mimic-transfected CSCs developed smaller spheres than control CSCs, showing the efficiency of hsa-miR-5688 in downregulating CSC's ability to form spheres. Interestingly, mimic + Dox-treated CSCs exhibited smallest sphere formation as compared to all the other sets, indicating least capacity of sphere formation collectively due to upregulated hsa-miR-5688 and Dox treatment, the latter generating additional stress in this hsa-miR-5688 upregulated but Dox-escaped CSCs.

Obtaining these results, next, we investigated the capacity of the CSCs of the aforementioned sets in establishing differentiated colonies under serum-containing conditions after removal of chemotherapy, simulating tumor-recurrence. For that, same numbers (1×10^4) of isolated CSCs from the previous experimental sets were propagated in serum-containing medium, to assess differentiation and colony formation capacity. After 72 h, Dox-treated CSCs developed the largest recurrent colonies in the differentiating medium than all the other sets, indicating that the "chemotherapy-strengthened" CSCs exhibited a higher recurrence potential following therapy withdrawal. Mimic-transfected CSCs generated smaller recurrent colonies in differentiating medium compared to the control set (Figure 8I), indicating that the upregulation of hsa-miR-5688 reduced CSC differentiation properties by downregulating *FOXC1*, thus resulting in impaired recurrent colony formation. Interestingly, mimic + Dox-treated CSCs produced the smallest recurrent colonies as compared to all other three sets within this stipulated time, demonstrating that these hsa-miR-5688-overexpressed CSCs were sensitized to Dox and furnished even lesser CSC-properties due to Dox treatment (Figure 8I). These findings indicated that while Dox alone greatly boosts CSCs' ability to promote tumor recurrence, hsa-miR-5688 upregulation not only inhibits the same but also sensitizes CSCs toward Dox. Most importantly, for those hsa-miR-5688-CSCs that could escape Dox-attack, their ability to form recurrent colonies by differentiating into NSCCs in the serum-containing media signifying tumor-recurrence potential gets significantly downregulated especially after Dox therapy.

Additionally, a multitude of reports has revealed that CK18 as a differentiation marker in breast cancer[50–52] and a study from our lab has also previously shown that CK18 expression was higher in cells and differentiated spheres while lower in secondary spheres.[53] In line with these reports, we next subjected the CSCs from the aforementioned experimental sets to serum-containing differentiation media, and evaluated their CK18 levels, to verify the differentiation potential of such CSCs into NSCCs, which may help the generation of recurrent tumor. Our results as evaluated by flow cytometry illustrated that CSCs from Dox-treated set, when subjected to the serum-containing differentiating medium, furnished the highest CK18 expression as compared to all the other sets, indicating that these CSCs had the greatest differentiation potential and recurrence-causing ability, following chemotherapy. CSCs isolated from the mimic set, on the other hand, expressed lesser CK18 than the control set in the differentiating medium (Figure S8B), indicating a diminished ability to cause recurrence. Finally, mimic + Dox-treated set expressed the least CK18 level in differentiating medium with respect to all the other three sets (Figure S8B), indicating a loss of differentiation capacity and a reduced ability to produce NSCCs, resulting in inhibition of tumor recurrence.

To further validate the contribution hsa-miR-5688-induced FOXC1 downregulation followed by tri-cycle chemotherapy, we compared the percentage of live CSCs in mimic and mimic + Dox-treated sets. Our results demonstrated that while transfection of mimic exhibited ~90 live CSCs, mimic + Dox treatment resulted in a significant decrease in the same thus showing ~20% live CSCs (Figure S8C).

It will not be out of context to mention here that although same numbers of CSCs were taken from both the sets, total live CSCs reduced in the mimic + Dox-treated set, along with significant reduction in sphere-formation and colony-generation ability of the mimic + Dox-treated CSCs when compared to the mimic-CSCs (Figures 8H and 8I). This further validated that the combinatorial treatment regime involving mimic and tri-cycle Dox not only kills CSCs but also remarkably hampers the recurrence potential of the remaining CSCs when compared to individual mimic- or Dox-treated sets.

In gist, these findings indicate that despite the completion of three Dox cycles, Dox did not only fail to trigger CSC apoptosis but additionally produced a FOXC1-pluripotency loop that guided FOXC1-modulated stemness along with drug resistance and also enabled development of the biggest spheres and colonies with the highest differentiation potential, after therapy removal. These findings signify not only Dox-stimulated increased potential of CSCs to escape death but also heightened CSC-features that might be responsible for higher recurrence in patients upon chemotherapy. Conversely, hsa-miR-5688 overexpression alone, although failed to produce substantial apoptosis in CSCs, resulted in the reduced expressions of FOXC1 and thereby reduced expression of stemness and drug-resistance markers, thus generating smaller spheres and colonies with reduced differentiation potential, emphasizing its contribution in inhibiting CSC-characteristics and possible tumor-recurrence. Furthermore, the efficiency of mimic treatment followed by chemotherapy was validated when mimic-sensitized CSCs not only furnished significant apoptosis upon Dox treatment, but these drug-escaped CSCs also generated the smallest spheres and colonies with the least differentiation potential in presence of serum-containing media, thus emphasizing its lowest recurrence capacity as compared to Dox or mimic alone, even though the same number of CSCs were taken. These results support the eligibility of hsa-miR-5688 for successfully targeting FOXC1, eventually decreasing CSC-characteristics and preventing breast cancer-recurrence when used in combination with chemotherapy.

Altogether this study unearthed a hitherto unknown mechanism where FOXC1 forms a reciprocal cross-regulation with pluripotency factors, OCT4 and SOX2, to increase the pool of CSCs by *trans*-activating not only OCT4 and SOX2 but also NANOG, and to ensure acquisition of resistance by transactivating the major drug-resistance factor ABCG2, in Dox-treated breast CSCs. Further exploration revealed sensitization of drug-resistant CSCs toward Dox upon ablation of FOXC1, *in-vivo* and in recurrence models. Finally, our pursuit established an inverse relationship between hsa-miR-5688 and FOXC1 in breast CSCs where overexpression of this miRNA sensitizes otherwise resistant breast CSCs toward Dox by repressing FOXC1, which in turn downregulates all the aforementioned stemness factors and drug-resistance marker ABCG2, to inhibit tumor recurrence after chemotherapy. These findings have significant implications for developing successful targeting of breast CSCs by utilizing hsa-miR-5688, thus ultimately assuring RFS of breast cancer patients.

DISCUSSION

Drug resistance poses a major threat to cancer therapy since most of the chemotherapeutic agents produce resistance after prolonged use. The recent notion portrays drug resistance in cancer as a multifaceted process. Understanding all aspects of this complicated process is, therefore, the main challenge in the field of cancer therapeutics. Development of cancer drug-resistance is thus a collective contribution of many targets and pathways.[54] Emergence of cancer stem cell theory implicates the continuous development of NSCCs from existing highly drug-resistant cancer-initiating stem cells after chemotherapy.[55] For combating drug resistance, it is thus necessary to consider the convergence of different aspects of resistance, and the contribution of CSCs in those. However, this important issue is often ignored when after chemotherapy the cancer patients become "clinically" cancer-free only to result in relapse after therapy withdrawal. Considering the multifaceted origin of drug-resistance, a combination of drugs/therapies might improve the outcome.[56–61] Here, we attempted to detect the effective "target" and the related pathways generating chemo-resistance, as well as the role of CSCs in controlling the same, to finally identify remedies for sensitization of drug-resistant cancer cells and the rationale to develop such therapies.

Recent studies have highlighted the emerging role of FOXC1 in the development, progression, and treatment resistance of several solid and liquid malignancies.[14,15,19,20,23,24] Indeed, in line with previous reports (refs),[62–64] our analysis also depicted that NACT-treated patients furnished increased expression of FOXC1 and were associated with poorer OS and RFS, in contrast to chemo-naive patients, thereby raising the possibility that chemotherapy-induced higher FOXC1 expression might serve as a marker for poor prognosis even after treatment. Since CSCs play key role in imparting therapy resistance thereby causing relapse post chemotherapy, previous information prompted us to investigate its involvement in breast CSCs. Our investigation revealed the existence of an intriguing reciprocal feedforward loop between FOXC1 and pluripotency factors, OCT4 and SOX2, in breast CSCs, which plays a pivotal role in promoting stemness and drug resistance during chemotherapy, allowing CSCs to survive and potentially repopulate the tumor after therapy withdrawal. Furthermore, FOXC1-ablation sensitized these resistant breast CSCs in both *in-vitro* and *in-vivo* models. Previous report demonstrating impaired CSC polarization and sensitization toward cisplatin and docetaxel upon FOXC1-ablation in NSCLC,[24] strengthened our findings and underscored the therapeutic potential of targeting FOXC1 in breast CSCs. Supporting our hypothesis, while Dox treatment alone not only failed to induce apoptosis in CSCs but also increased stemness, it effectively reduced tumor volume by killing NSCCs, the major subpopulation of cells of the tumor mass. Interestingly, since FOXC1-ablation in CSCs decreased the expression of pluripotency and drug-resistant factors due to disruption of the feedforward loop, the transfectants were lesser tumorigenic[65–67] and furnished least tumor volume upon Dox treatment, thereby signifying that the downregulation of FOXC1 was sufficient to inhibit Dox-induced upregulation of pluripotency and drug-resistant factors and thereby related tumor development. These findings

highlighted the central role of FOXC1 in regulating stemness and drug resistance, and suggested that targeting FOXC1 could hinder chemotherapy-induced generation of "aggravated" CSC phenotype, thereby finally contributing to tumor regression.

NACT is a cornerstone of breast cancer treatment, yet it increases CSC number[38] thereby posing a significant risk of recurrence at local and also at secondary sites due to their ability to migrate and sustain distant tumor growth[68] in patients with residual invasive cancer post-chemotherapy, which can adversely affect overall life expectancy.[69] Although chemotherapy is typically administered in multiple cycles,[70] tri-cycle Dox chemotherapy has been reported to enrich breast CSC population.[71] In line with these reports, in our *in-vitro* model, tri-cycle Dox-therapy indeed increased the recurrence potential of CSCs as compared to untreated CSCs, highlighting the role of chemotherapy in promoting CSC enrichment and tumor recurrence. Here again, FOXC1-ablation in combination with Dox, resulted in a decrease in recurrence potential, suggesting a critical role of FOXC1 in ensuring CSC survival during chemotherapy, possibly by upregulating drug-resistance pump ABCG2 and induce the stemness genes through the aforementioned reciprocal feedforward loop, thereby ensuring CSC survival and tumor relapse after chemotherapy. Most importantly, attenuation of FOXC1 inhibited tumor recurrence post three-cycle chemotherapy, which was not achievable by Dox treatment or FOXC1-ablation alone. These findings were corroborated by our mouse model experiments, emphasizing the candidacy of FOXC1 as an essential therapeutic target in breast cancer.

The aforementioned discussion tempted us to identify putative drug molecule, which can target FOXC1 thereby in combination with chemotherapy might regress breast cancer. In this regard, microRNAs (miRNAs) have garnered significant attention in cancer diagnostics and therapeutics due to their regulatory roles in gene expression.[26,28,29,35,48] Alterations in miRNA levels during NACT have been implicated in predicting pathological complete response in triple negative breast cancer,[72] highlighting their potential as biomarkers for treatment response. Recent report demonstrated that miR-495 inhibits cell proliferation and promotes apoptosis in endometrial cancer by repressing FOXC1 expression.[30] Similarly, overexpression of miR-200 in breast CSCs disrupts colony formation and reduces carcinogenesis,[73] underscoring the therapeutic potential of miRNA-based strategies in cancer. Our search for identifying FOXC1-targetting miRNA revealed hsa-miR-5688 as a less-investigated miRNA with potential implications in breast cancer prognosis and therapy. Supporting the candidature of this miRNA, we observed higher probability of OS of breast cancer patients with higher expression of hsa-miR-5688.[49] In fact, hsa-miR-5688 expression is significantly lower in CSCs compared to NSCCs, which suggest its probable role in regulating CSC properties. Indeed, upregulation of hsa-miR-5688 led to FOXC1 downregulation, resulting in reduced stemness and resistance in CSCs thereby increasing sensitivity of CSCs to chemotherapy. Such attenuated expression of hsa-miR-5688 in breast CSCs led us to hypothesize that this might be an adaptive mechanism of these highly resistant cells to evade the anti-FOXC1 effect of this micro-RNA, thereby promoting CSC survival and therapy resistance and signifying its critical role in repressing FOXC1-mediated stemness and drug resistance. Validating our hypothesis, Dox-treated CSCs furnished enhanced differentiation potential when subjected to serum-containing media, thereby, indicating high recurrence capability of such CSCs, after withdrawal of the drug. In contrast, augmentation of hsa-miR-5688 prior to Dox treatment effectively suppressed differentiation capacity, highlighting the efficacy of this miRNA to reduce differentiation of the drug-spared CSCs, if any, to tumor-mass forming NSCCs, thereby hindering recurrence of breast cancer after chemotherapy.

To summarize, this report revealed a novel understanding of chemotherapeutic escape of CSCs and the role of FOXC1 in it. Chemotherapy-driven FOXC1 initiates a reciprocal feedforward transactivation loop that serves as a master regulator of the stemness and drug-resistant factors in breast CSCs thus helping these cells escape death. Sensitizing CSCs by FOXC1-ablation make CSCs vulnerable, thus lowering recurrence. Our findings further suggested that hsa-miR-5688 downregulates FOXC1 thus hindering chemotherapy-induced further gain in stemness, drug-resistance and recurrence. Thus, integrating hsa-miR-5688 therapy with chemotherapy might prove to be a successful regimen to reduce burden in breast cancer patients as well as improve their long-term survival.

Previous discussion signifies that the efficacious management of cancer depends on two critical issues, (1) proper selection of the modality of the therapy, and (2) prevention of relapse. During past few decades, there is much advancement in therapy but the issue of relapse has still remained unconquered. Our findings not only identified target in CSCs but also the targeting molecule, both of which are relevant toward reducing the rate of cancer relapse, as well as the development of improved combination therapies. Although inhibitors of many known targets are either already in use or in the development process, it is frustrating that almost all of them generate resistance. Here, we portray a combination therapy for which a miRNA that already exists in the cells, can be used in combination with chemotherapy, for combating cancer effectively while significantly reducing relapse.

MATERIALS AND METHODS

Cell culture

MDA-MB-468, MDA-MB-231, MCF-7, and 4T1 breast cancer cell lines were procured from the National Centre for Cell Science, Pune, India, with their respective STR profiles and cell-line authentication certificates. After resuscitation, none of the cell lines were passaged for more than six months. According to earlier descriptions, cells were consistently maintained in complete RPMI and DMEM media in a humidified incubator at 37°C with 5% CO_2.[53,74] Cell confluence was allowed before usage.

Sphere culture

Cells were seeded at 2.5×10^4 cells per well in six well ultra-low adherence plates (Corning) for sphere culture in Dulbecco's

modified Eagle's medium/F12 medium supplemented with basic fibroblast growth factor (20 ng/mL), bovine insulin (5 μg/mL) (Sigma-Aldrich), B27 supplement (BD Biosciences), 0.4% bovine serum albumin (BSA), and recombinant epidermal growth factor (20 ng/mL) as mentioned previously.[53,74] Weekly trypsinization and dissociation of primary (1^0) spheres (% CSC) were followed by reseeding in SFM at 2.5×10^4 cells per well in ultra-low-adherence six-well plates for secondary (2^0) sphere (% CSC) formation.

Sorting of pure CSCs and NSCCs

Breast cancer 2^0 spheres were disaggregated into single-cell suspension by pipetting and passing through 30-μm nylon mesh; 1×10^7 cells were mixed with CD24-Biotin followed by anti-Biotin microbeads (Mitenyi Biotec). The cell suspension was loaded onto the magnetic column. The $CD24^+$ cells were retained on the column while $CD24^-$ fraction passed through the column in the flowthrough. These two fractions of $CD24^-$ and $CD24^+$ cells were next mixed with CD44 microbeads (Mitenyi Biotec) and again loaded onto the magnetic column and collection of different cell fractions finally led to the isolation of $CD44^+/CD24^-$ as CSC subpopulation and $CD44^-/CD24^-$, $CD44^-/CD24^+$, and $CD44^+/CD24^+$ as NSCC subpopulation.

cDNA synthesis, semiquantitative, and quantitative real-time PCR

TRIzol reagent (Ambion) was used to extract total RNA from cells and 1 μg of that was reverse transcribed using cDNA Synthesis kit (Takara Bio) before being subjected to semiquantitative PCR with Taq (Takara Bio) using GeneAmp-PCR System 2720 (Applied Biosystems) or real-time PCR with SYBR Green Master mix (Takara Bio/Roche) in Roche Light Cycler 96 system. U6-RT Stem and hsa-miR-5688 Stem oligonucleotides listed in Table S1 were utilized to synthesize miRNA cDNAs. Primers described in Table S1 were used to amplify the cDNAs. Semiquantitative PCR products were analyzed by 2% agarose gel electrophoresis. Fold change was computed for real-time PCR using the ΔΔCt technique with $2^{-\Delta\Delta Ct}$.[53]

Western blot

For preparation of whole cell lysates, CSCs and NSCCs were homogenized in lysis buffer (20 mM HEPES [pH7.5], 1.5 mM MgCl2, 10 mM KCl, 1 mM dithiothreitol, and 1 mM Na-EDTA). Protease inhibitor combinations were added to all buffers (Thermo Fisher Scientific). The Lowry technique was used to calculate protein concentrations. Lysates containing 60–100 μg of protein were combined with an equivalent amount of 2X SDS-PAGE sample buffer, heated for 2 min at 100°C, and loaded onto a 10% SDS-PAGE gel (depending on the molecular weight of the protein of interest). Each well received an equal quantity of protein. Before antibody treatments, the proteins were transferred to a poly-vinylidene difluoride membrane (Merck Millipore), which was subsequently blocked with 5% (w/v) non-fat dried milk in tris-buffered saline with 0.05% (v/v) Tween 20. The membranes were probed with appropriate primary antibodies, followed by HRP-tagged secondary antibodies, and visualized by chemiluminescence. The antibodies used are FOXC1 (Novus Biologicals, Thermo Fisher Scientific), SOX2 and OCT4 (Cell Signaling Technology). Equivalent protein loading was verified using β-Actin (Cell Signaling Technology).[53] Densitometric scanning was performed using Image Lab software, Bio-Rad.

Chromatin immunoprecipitation

Millipore's standard procedure was used for the ChIP assays. PCR was used for the detection of OCT4 binding site on FOXC1 promoter. ChIP assays were also performed for identification of FOXC1 binding site on OCT4, SOX2, NANOG, and ABCG2 promoters. List of ChIP primers have been shown in Table S1. The DNA extracted was employed in semiquantitative or real-time PCR experiments. Semiquantitative PCR products were analyzed by 2% (w/v) agarose gel electrophoresis. Fold change was computed for real-time PCR using the ΔΔCt technique with $2^{-\Delta\Delta Ct}$.[53]

Lentiviral-mediated FOXC1-shRNA transduction

Transient transfection of HEK cells was used to package lentiviruses. HEK cells were seeded in a T75 flask one day before transfection at 1×10^5 cells/cm^2 in DMEM (high glucose) supplemented with 40 mg/mL gentamicin, 10% FCS, and 1 mM pyruvate. Cells were co-transfected with 7.5-μg gag/pol packaging plasmid psPAX2, 7.5-μg FOXC1-shRNA (abm goods) lentiviral vector/control-scramble (addgene), and 4-μg envelope plasmid pMD2.G utilizing the Profection mammalian transfection system (Promega) via the calcium phosphate precipitation method. A 10-mL DMEM without antibiotics was used for performing transfections and cultured for 16 h. Thereafter every 24 and 48 h, the media was changed with completely supplemented DMEM and supernatant was collected. Cell debris was eliminated using centrifugation at 4 °C at 1500 rpm for 5 min and later passing through 0.45-μm pore PES filter; 20 mL of supernatant combined with polyethylene-glycol (PEG-8000) in 1X PBS was used to achieve a final concentration of 12% and centrifuged for 20 min at 4000 rpm at 4°C. Virus pellets were resuspended in serum, antibiotic-free DMEM. Aliquots were kept at −80°C. MDA-MB-468 CSCs and 4T1 2^0 spheres were transduced with either scramble lentiviral vector or FOXC1-shRNA lentiviral vectors at a multiplicity of infection of 1×10^7 transducing units per ml in the presence of polybrene (8 μg/mL).[75]

Plasmids and transfections

OCT4-shRNA (addgene), SOX2-shRNA (addgene), FOXC1-shRNA (abm goods), control-scramble-shRNA (addgene), and hsa-miR-5688 mimic (Sigma) were transfected using Lipofectamine-2000 (Invitrogen) following manufacturer's protocol. 2′-O-methyl RNA oligonucleotide hsa-miR-5688 decoy was synthesized by IDT,[76] and Lipofectamine-2000 was also used to transfect cells. These cells were collected after 34 to 36 h to evaluate knockdown effectiveness by RT-PCR.[36,53]

Treatment of CSCs

To assess the effect of chemotherapy on cells, mammospheres, and sorted CSCs, they were treated with chemotherapeutic agent Dox (MP Biomedicals) (2.5 μM) for 24 h.[36,53]

Relapse

The 1^0 spheres of MDA-MB-468 were divided into six sets: (1) control (scramble-shRNA), (2) Dox-treated, (3) FOXC1-shRNA-transfected, (4) FOXC1-shRNA-transfected + Dox-treated, (5) mimic-transfected, and (6) mimic-transfected + Dox-treated. Only sets (2), (4), and (6) were treated with Dox (2.5 μM) (MP Biomedicals) for 24 h. Next, the medium was discarded and replaced with complete media for 48 h. This was one complete cycle whose total time period was 72 h which was repeated another two times for a total of three cycles. After each cycle, samples from each experimental set were analyzed by flow cytometry for percentage apoptosis (annexin-V-FITC$^+$) of these sets. Additionally, after completion of the third cycle, samples from all the experimental sets were MACS sorted to obtain pure CSCs and analyzed for relative expression (MFI) FOXC1, stemness factors OCT4, SOX2, and NANOG as well as drug-resistance marker ABCG2. In addition, after the last cycle, samples from all the experimental sets (1×10^4) of sorted CSCs were counted and further seeded in 24-well plate in SFM for sphere formation assay for 7 days and also in 24 well-plate containing serum for colony formation for 72 h which were visualized via phase contrast microscope (Leica) and area of the colonies were measured using ImageJ software.

Primary human tissue samples

Human primary breast cancer patient-derived tissue samples were collected ($n = 5$) with informed consent from the Department of Surgery, IPGMER and SSKM Hospital, Kolkata, India, in compliance with the recommendations of the Research Oversight Committee of IPGMER. All related studies and analysis were performed at Bose Institute, Kolkata, India, in compliance with the Institutional Human Ethics Committee (BIHEC/2017-18/5). These tumors were all primary site cancers. Inclusion criteria for the study were female patients of 18–65 years of age, diagnosed with breast cancer (BC) with known ER/PR/HER2 status as indicated in Table S2. Unavailability of known ER/PR/HER2 status of the patients was considered as exclusion criteria. Tissues were collected and processed by MACS sorting into pure CSCs and NSCCs. The tissues were mechanically disaggregated, collagenase digested, as well as filtered through a 30-μm filter before sorting.[77] CD44$^+$/CD24$^-$ fraction was the CSC subpopulation while CD44$^-$/CD24$^-$, CD44$^-$/CD24$^+$, and CD44$^+$/CD24$^+$ fractions were the NSCC subpopulation. These fractions were further subjected to RNA isolation, cDNA synthesis, and real-time PCR.

Flow cytometry

Flow cytometric analysis of CD44-APC (human, mouse) and CD24-PE (human, mouse) antibodies (BD Biosciences) was used to analyze the expression of breast CSC markers CD44 and CD24. P2-CSC population (CD44$^+$/CD24$^-$) was gated from the P1 parent population, and P3-NSCC population (CD44$^+$/CD24$^+$, CD44$^-$/CD24$^-$, CD44$^-$/CD24$^+$) was also gated from P1 parent population. Flow cytometry was performed to quantify the percentage of apoptosis using the FITC-annexin V apoptosis detection kit (BD Biosciences) following manufacturer's protocol. The antibodies used for determining the relative (MFI's) are FOXC1-untagged (Novus Biologicals, Thermo Fisher Scientific); ALDH1-Alexa Fluor 488, MDR1-untagged, MRP1-untagged (Santa Cruz); ABCG2-FITC, OCT4-Percp Cy 5.5, NANOG-PE, SOX2-APC (BD Biosciences); and anti-goat Alexa Fluor 488, 546; anti-mouse Alexa Fluor 488, 546; and anti-rabbit Alexa Fluor 488, 546 (Invitrogen).[53]

For staining of cell surface markers (CD44, CD24, MDR1, MRP1, and ABCG2), samples were washed in 1X PBS and fixed with cytofix buffer (BD Biosciences), followed by incubation with respective antibodies for 30 min. For staining of intra-cellular transcription factors, OCT4, SOX2, and NANOG, BD Stemflow Pluripotent Stem Cell Transcription Factor Analysis Kit (BD Biosciences) was used as per the manufacturer's protocol Moreover, for staining intracellular marker FOXC1 and ALDH1, samples were firstly washed, fixed, and permeabilized with the cytofix and cytoperm buffer combination (BD Biosciences) and, then, incubated with respective antibodies. For example, intracellular FOXC1 protein was stained with anti-FOXC1 antibody for 45–60 min, followed by counterstaining with Alexa Fluor 488 for 30 min. For staining of intracellular ALDH1, Alexa Fluor 488-tagged anti-ALDH1 antibody was used. Data were collected using BD FACSVerse and were analyzed using BD FACSVerse Suite software (BD Biosciences).[78]

Animal experiments

Female BALB/c mice harboring syngeneic breast cancer 4T1 cell line was utilized to investigate the role of Foxc1 in controlling tumor formation *in-vivo*. Female BALB/c mice weighing 20–25 g were housed in a temperature-controlled, light-dark cycle environment. All animal studies were carried out following laboratory animal care norms (NIH publication no. 85-23, revised in 1985) and Indian laws on "Protection of Animals" under the supervision and control of Bose Institute's ethics committee (reg. no. 95/99/CPCSEA; approval no: IAEC/BI/130/2019). The following experiment was performed using BALB/c mice: Foxc1-shRNA/control-scramble was stably transfected in murine breast cancer cell line 4T1. The cells bearing Foxc1-shRNA/control-scramble shRNA were selected using puromycin for several passages to obtain pure population of Foxc1-shRNA/control-scramble shRNA-bearing 4T1 cells and the same number of control and Foxc1-shRNA 4T1 cells was subjected to sphere formation. Next, BALB/c mice were divided into two sets: (1) inoculated with control 4T1 2^0 spheres (1×10^6 single cells), and (2) inoculated with same number of Foxc1-shRNA 4T1 2^0 spheres (1×10^6 single cells). After appearance of tumors (7 days) in the mice, the tumor volumes were determined every 2 days for 14 days. Next, each of the previous sets were subdivided into two more sets: (1) control and (2) Dox-treated. One week after tumor formation, chemotherapy-treatment set were intraperitoneally injected with 5 mg/kg Dox, every alternate day for 15 days after which the mice were sacrificed, and tumor images were taken and tumor volume was measured. Percentage of CD44$^+$/CD24$^-$ CSCs was estimated in each set of tumors by flow cytometry, while expression of *Foxc1*, *Oct4*, *Sox2*, *Nanog*, and *Abcg2* was measured by RT-PCR.[53]

Molecular docking and modeling of protein-DNA complexes

The complete, AlphaFold modeled, 3D structures of OCT4, SOX2, and FOXC1 transcription factors were already available in the AlphaFold database (AFDB accession IDs in Tables S3 and S4). To model the protein-DNA interactions, the protein coordinate was first downloaded from AlphaFold database and then the structure was processed in PyMOL[79] to extract the essential DBDs. The B-form DNA coordinates of the respective promoter sequences were generated using W3DNA webserver.[80] To generate the complexes, the modeled promoter sequences were then docked with the DBDs of the respective transcription factors, as described in Tables S3 and S4, using HADDOCK (High Ambiguity Driven protein-protein Docking) webserver[81] (version 2.4) that followed a flexible docking approach. The residues of FOXC1, OCT4, and SOX2 that were potentially involved in DNA interactions were identified from previous experimental reports[44,82,83] and were used as active residues for site-specific docking (Tables S3 and S4); the remaining residues of the proteins were automatically defined as passive ones. These residue definitions were used to generate Ambiguous interaction restraints (AIR) during the docking process. The docked protein-DNA complexes were briefly energy minimized to eliminate the steric clashes from the model and those optimized structures were then inspected and analyzed in PyMOL.

Expression, survival, correlation, and putative FOXC1-miRNA target analyses

To investigate the relationship between FOXC1 and chemotherapy in breast cancer, we first divided the breast cancer patient data from publicly available datasets (GSE69031 and GSE28844) into two cohorts, chemo-naive (untreated) (n = 31 for GSE69031 and n = 31 for GSE28844) and chemotherapy-treated patients (n = 26 for GSE69031 and n = 29 for GSE28844), and examined FOXC1 mRNA expression in both.[39] Furthermore, we have used the endpoint data from GSE69031 and GSE28844 datasets to predict RFS and event-free survival, respectively of the chemo-treated breast cancer patients using R2: Genomics Analysis and Visualization Platform database. Next, we correlated the FOXC1 mRNA level with disease prognosis in breast cancer patients by analyzing Kaplan-Meier (Km) plots using the publicly available Km plotter database.[40] For the same, we divided the patients into two groups, i.e., (1) chemo-naïve (untreated), and (2) NACT, and analyzed their OS and RFS relative to FOXC1 mRNA expression (Reporter ID - 213260_at). Additionally, we evaluated FOXC1 correlation with stemness factors OCT4, SOX2, NANOG, and drug-resistance markers ABCG2, MRP1, MDR1 from the publicly available R2 database microarray dataset GSE25066 (n = 508) using *FOXC1* (Reporter ID: 213260_at), *OCT4* (Reporter ID: 208286_x_at), *SOX2* (Reporter ID: 214178_s_at), *NANOG* (Reporter ID: 220184_at), *ABCG2* (Reporter ID: 209735_at), *MRP1* (Reporter ID: 202805_s_at), and *MDR1* (Reporter ID: 209994_s_at).[40] Moreover, association between FOXC1 (Reporter ID: 213260_at) and *OCT4* (Reporter ID: 214532_x_at) among chemo-naive and chemo-treated breast cancer patients were evaluated using GSE69031 dataset from R2: Genomics Analysis and Visualization Platform database. Km plot of OS of triple negative breast cancer patients with hsa-miR-5688 expression was also analyzed.[40] Finally, miRNAs with putative FOXC1 binding sites were identified using Mir-Carta and DIANA tools databases with micro-T CDS score cut-off >0.95 have been listed in Table S5 with miRNAs that have not been explored much shown in red.[47,48]

Promoter analysis

The −2000 bp to +100 bp spanning promoter sequences of human FOXC1, OCT4, SOX2, NANOG, and ABCG2 genes were obtained from the EPD[41,42]. The OCT4 binding site on FOXC1 promoter and SOX2 binding site on FOXC1 promoter as well as FOXC1 binding sites on OCT4, SOX2, NANOG, and ABCG2 promoters were identified using JASPAR transcription factor binding profile database.[43]

Statistical analysis

Unless otherwise specified, values are presented as mean and standard error. GraphPad Prism version 8.00 was used to create all quantitative figures, with the alpha level set at 0.05 for all experiments. Each of the experiments was independently performed at least three times, data were analyzed, and statistical significance ($p < 0.05$) of mean value differences was evaluated using appropriate statistical tests. Unpaired Student's t test was done for statistical analysis.

DATA AVAILABILITY

The datasets generated during the current study are available with the corresponding author.

ACKNOWLEDGMENTS

The authors are grateful to the Indian Council of Medical Research (ICMR) for providing ICMR Emeritus Scientist-ships to T.D. (74/1/2020-Pers) and G.S. (HRD/Head/IES/2023) and to the Bioinformatics Center Project of S.G.D. at Bose Institute funded by DBT (BT/PR40174/BTIS/137/45/2022). The authors also acknowledge Prof. Kaushik Biswas, Unified Academic Campus, Bose Institute, for his thoughtful comments on this manuscript. The authors thank R. Dutta and S. Das of Bose Institute, Kolkata, for their technical assistance.

This work was supported by research grants from Indian Council of Medical Research (IES scheme nos. 74/1/2020-Pers and HRD/Head/IES/2023), Department of Science and Technology–Science and Engineering Research Board (DST-SERB), and Government of India (EMR/2016/003607). Support grants were received from University Grants Commission (A.D., A.B., D.G., and S.B.), Council of Scientific and Industrial Research (S.C., S.M., and N.R.C.), Department of Science and Technology (S.P.), and Department of Science and Technology—Science and Engineering Research Board (U. B.), India.

Human primary breast cancer tissue specimens were collected with informed consent from patients of Department of Surgery, IPGMER and SSKM hospital, Kolkata, India, in compliance with the recommendations of the Research Oversight Committee of IPGMER, and all related studies and analysis were performed at Bose Institute, Kolkata, India, in compliance with the Institutional Human Ethics Committee (BIHEC/2017-18/5).

This study was performed in line with the principles of laboratory animal care norms (NIH publication no. 85-23, revised in 1985) and Indian laws on "Protection of Animals" under the supervision and control of Bose Institute's ethics committee (reg. no. 95/99/CPCSEA; approval no. IAEC/BI/130/2019).

AUTHOR CONTRIBUTIONS

Conception and design: T.D. Background literature study, development of methodology, and preparation of the manuscript: A.D., S.C., and T.D. Acquisition of data: Tissue culture, RNA isolation, cDNA preparation, real-time qPCR , ChIP assays, flow cytometry etc.: A.D., S.C., A.B., U.B., and S.M. *In-silico* miRNA database mining and related experiments: S.P. and D.G. Microscopy experiments: S.B.; docking experiments: N.R.C. and S.G.D. *In-vivo* mice experiments: K.J. Primary human breast tissue-related experiments: A.D., A.B., S.C., and D.K.S. Analysis and interpretation of data: A.D., S.C., G.S., S.G.D., and T.D. Review of the figures and manuscript editing: G.S. and S.G.D. The final review: T.D. Administrative, technical, or material support: T.D. The manuscript has been approved by all authors.

DECLARATION OF INTERESTS

The authors declare no competing interests.

SUPPLEMENTAL INFORMATION

Supplemental information can be found online at https://doi.org/10.1016/j.omton.2025.200982.

REFERENCES

1. Al-Hajj, M., Wicha, M.S., Benito-Hernandez, A., Morrison, S.J., and Clarke, M.F. (2003). Prospective identification of tumorigenic breast cancer cells. Proc. Natl. Acad. Sci. USA *100*, 3983–3988. https://doi.org/10.1073/pnas.0530291100.
2. Yu, Z., Pestell, T.G., Lisanti, M.P., and Pestell, R.G. (2012). Cancer stem cells. Int. J. Biochem. Cell Biol. *44*, 2144–2151. https://doi.org/10.1016/j.biocel.2012.08.022.
3. Phi, L.T.H., Sari, I.N., Yang, Y.-G., Lee, S.-H., Jun, N., Kim, K.S., Lee, Y.K., and Kwon, H.Y. (2018). Cancer Stem Cells (CSCs) in Drug Resistance and their Therapeutic Implications in Cancer Treatment. Stem Cells Int. *2018*, 5416923. https://doi.org/10.1155/2018/5416923.
4. Mitra, A., Mishra, L., and Li, S. (2015). EMT, CTCs and CSCs in tumor relapse and drug-resistance. Oncotarget *6*, 10697–10711. https://doi.org/10.18632/oncotarget.4037.
5. Zhao, W., Li, Y., and Zhang, X. (2017). Stemness-Related Markers in Cancer. Cancer Transl. Med. *3*, 87–95. https://doi.org/10.4103/ctm.ctm_69_16.
6. Li, Y., Wang, Z., Ajani, J.A., and Song, S. (2021). Drug resistance and Cancer stem cells. Cell Commun. Signal. *19*, 19. https://doi.org/10.1186/s12964-020-00627-5.
7. Nathansen, J., Meyer, F., Müller, L., Schmitz, M., Borgmann, K., and Dubrovska, A. (2021). Beyond the Double-Strand Breaks: The Role of DNA Repair Proteins in Cancer Stem-Cell Regulation. Cancers *13*, 4818. https://doi.org/10.3390/cancers13194818.
8. Liu, L., Yang, L., Yan, W., Zhai, J., Pizzo, D.P., Chu, P., Chin, A.R., Shen, M., Dong, C., Ruan, X., et al. (2018). Chemotherapy Induces Breast Cancer Stemness in Association with Dysregulated Monocytosis. Clin. Cancer Res. *24*, 2370–2382. https://doi.org/10.1158/1078-0432.CCR-17-2545.
9. Mansoori, B., Mohammadi, A., Davudian, S., Shirjang, S., and Baradaran, B. (2017). The Different Mechanisms of Cancer Drug Resistance: A Brief Review. Adv. Pharm. Bull. *7*, 339–348. https://doi.org/10.15171/apb.2017.041.
10. Tada, Y., Wada, M., Migita, T., Nagayama, J., Hinoshita, E., Mochida, Y., Maehara, Y., Tsuneyoshi, M., Kuwano, M., and Naito, S. (2002). Increased expression of multidrug resistance-associated proteins in bladder cancer during clinical course and drug resistance to doxorubicin. Int. J. Cancer *98*, 630–635. https://doi.org/10.1002/ijc.10246.
11. Bukowski, K., Kciuk, M., and Kontek, R. (2020). Mechanisms of Multidrug Resistance in Cancer Chemotherapy. Int. J. Mol. Sci. *21*, 3233. https://doi.org/10.3390/ijms21093233.
12. Hannenhalli, S., and Kaestner, K.H. (2009). The evolution of Fox genes and their role in development and disease. Nat. Rev. Genet. *10*, 233–240. https://doi.org/10.1038/nrg2523.
13. Ray, P.S., Wang, J., Qu, Y., Sim, M.-S., Shamonki, J., Bagaria, S.P., Ye, X., Liu, B., Elashoff, D., Hoon, D.S., et al. (2010). FOXC1 Is a Potential Prognostic Biomarker with Functional Significance in Basal-like Breast Cancer. Cancer Res. *70*, 3870–3876. https://doi.org/10.1158/0008-5472.CAN-09-4120.
14. Wang, J., Ray, P.S., Sim, M.-S., Zhou, X.Z., Lu, K.P., Lee, A.V., Lin, X., Bagaria, S.P., Giuliano, A.E., and Cui, X. (2012). FOXC1 regulates the functions of human basal-like breast cancer cells by activating NF-κB signaling. Oncogene *31*, 4798–4802. https://doi.org/10.1038/onc.2011.635.
15. Xia, L., Huang, W., Tian, D., Zhu, H., Qi, X., Chen, Z., Zhang, Y., Hu, H., Fan, D., Nie, Y., and Wu, K. (2013). Overexpression of forkhead box C1 promotes tumor metastasis and indicates poor prognosis in hepatocellular carcinoma. Hepatology *57*, 610–624. https://doi.org/10.1002/hep.26029.
16. Grivennikov, S.I., Greten, F.R., and Karin, M. (2010). Immunity, Inflammation, and Cancer. Cell *140*, 883–899. https://doi.org/10.1016/j.cell.2010.01.025.
17. Nagel, S., Ehrentraut, S., Meyer, C., Kaufmann, M., Drexler, H.G., and MacLeod, R.A.F. (2014). Oncogenic deregulation of NKL homeobox gene MSX1 in mantle cell lymphoma. Leuk. Lymphoma *55*, 1893–1903. https://doi.org/10.3109/10428194.2013.864762.
18. Nagel, S., Meyer, C., Kaufmann, M., Drexler, H.G., and MacLeod, R.A.F. (2014). Deregulated FOX genes in Hodgkin lymphoma. Genes Chromosomes Cancer *53*, 917–933. https://doi.org/10.1002/gcc.22204.
19. Somerville, T.D.D., Wiseman, D.H., Spencer, G.J., Huang, X., Lynch, J.T., Leong, H.S., Williams, E.L., Cheesman, E., and Somervaille, T.C.P. (2015). Frequent Derepression of the Mesenchymal Transcription Factor Gene FOXC1 in Acute Myeloid Leukemia. Cancer Cell *28*, 329–342. https://doi.org/10.1016/j.ccell.2015.07.017.
20. Ray, P.S., Bagaria, S.P., Wang, J., Shamonki, J.M., Ye, X., Sim, M.-S., Steen, S., Qu, Y., Cui, X., and Giuliano, A.E. (2011). Basal-Like Breast Cancer Defined by FOXC1 Expression Offers Superior Prognostic Value: A Retrospective Immunohistochemical Study. Ann. Surg Oncol. *18*, 3839–3847. https://doi.org/10.1245/s10434-011-1657-8.
21. Takebe, N., Miele, L., Harris, P.J., Jeong, W., Bando, H., Kahn, M., Yang, S.X., and Ivy, S.P. (2015). Targeting Notch, Hedgehog, and Wnt pathways in cancer stem cells: clinical update. Nat. Rev. Clin. Oncol. *12*, 445–464. https://doi.org/10.1038/nrclinonc.2015.61.
22. Hayashi, H., and Kume, T. (2008). Foxc Transcription Factors Directly Regulate Dll4 and Hey2 Expression by Interacting with the VEGF-Notch Signaling Pathways in Endothelial Cells. PLoS One *3*, e2401. https://doi.org/10.1371/journal.pone.0002401.
23. Han, B., Qu, Y., Jin, Y., Yu, Y., Deng, N., Wawrowsky, K., Zhang, X., Li, N., Bose, S., Wang, Q., et al. (2015). FOXC1 Activates Smoothened-Independent Hedgehog Signaling in Basal-like Breast Cancer. Cell Rep. *13*, 1046–1058. https://doi.org/10.1016/j.celrep.2015.09.063.
24. Cao, S., Wang, Z., Gao, X., He, W., Cai, Y., Chen, H., and Xu, R. (2018). FOXC1 induces cancer stem cell-like properties through upregulation of beta-catenin in NSCLC. J. Exp. Clin. Cancer Res. *37*, 220. https://doi.org/10.1186/s13046-018-0894-0.
25. MacFarlane, L.-A., and Murphy, P.R. (2010). MicroRNA: Biogenesis, Function and Role in Cancer. Curr. Genomics *11*, 537–561. https://doi.org/10.2174/138920210793175895.
26. Bader, A.G., Brown, D., and Winkler, M. (2010). The Promise of MicroRNA Replacement Therapy. Cancer Res. *70*, 7027–7030. https://doi.org/10.1158/0008-5472.CAN-10-2010.
27. Shah, M.Y., Ferrajoli, A., Sood, A.K., Lopez-Berestein, G., and Calin, G.A. (2016). microRNA Therapeutics in Cancer — An Emerging Concept. EBioMedicine *12*, 34–42. https://doi.org/10.1016/j.ebiom.2016.09.017.
28. Ebert, M.S., and Sharp, P.A. (2010). MicroRNA sponges: Progress and possibilities. RNA *16*, 2043–2050. https://doi.org/10.1261/rna.2414110.
29. Stenvang, J., Petri, A., Lindow, M., Obad, S., and Kauppinen, S. (2012). Inhibition of microRNA function by antimiR oligonucleotides. Silence *3*, 1. https://doi.org/10.1186/1758-907X-3-1.
30. Xu, Y.-Y., Tian, J., Hao, Q., and Yin, L.-R. (2016). MicroRNA-495 downregulates FOXC1 expression to suppress cell growth and migration in endometrial cancer. Tumor Biol. *37*, 239–251. https://doi.org/10.1007/s13277-015-3686-6.
31. Zhou, Y., Liu, S., Wang, W., Sun, Q., Lv, M., Yang, S., Tong, S., and Guo, S. (2021). The miR-204-5p/FOXC1/GDF7 axis regulates the osteogenic differentiation of human adipose-derived stem cells via the AKT and p38 signalling pathways. Stem Cell Res. Ther. *12*, 64. https://doi.org/10.1186/s13287-020-02117-4.

32. Peng, Y., and Croce, C.M. (2016). The role of MicroRNAs in human cancer. Sig. Transduct. Target Ther. *1*, 15004–15009. https://doi.org/10.1038/sigtrans.2015.4.

33. Lu, J., Getz, G., Miska, E.A., Alvarez-Saavedra, E., Lamb, J., Peck, D., Sweet-Cordero, A., Ebert, B.L., Mak, R.H., Ferrando, A.A., et al. (2005). MicroRNA expression profiles classify human cancers. Nature *435*, 834–838. https://doi.org/10.1038/nature03702.

34. Chung, T.K., Lau, T.S., Cheung, T.H., Yim, S.F., Lo, K.W., Siu, N.S., Chan, L.K.Y., Yu, M.Y., Kwong, J., Doran, G., et al. (2012). Dysregulation of microRNA-204 mediates migration and invasion of endometrial cancer by regulating FOXC1. Int. J. Cancer *130*, 1036–1045. https://doi.org/10.1002/ijc.26060.

35. Lee, S.W.L., Paoletti, C., Campisi, M., Osaki, T., Adriani, G., Kamm, R.D., Mattu, C., and Chiono, V. (2019). MicroRNA delivery through nanoparticles. J. Control. Release *313*, 80–95. https://doi.org/10.1016/j.jconrel.2019.10.007.

36. Banerjee, S., Mukherjee, S., Bhattacharya, A., Basak, U., Chakraborty, S., Paul, S., Khan, P., Jana, K., Hazra, T.K., and Das, T. (2020). Pyridoxine enhances chemoresponsiveness of breast cancer stem cells *via* redox reconditioning. Free Radic. Biol. Med. *152*, 152–165. https://doi.org/10.1016/j.freeradbiomed.2020.02.031.

37. Mukherjee, S., Adhikary, S., Gadad, S.S., Mondal, P., Sen, S., Choudhari, R., Singh, V., Adhikari, S., Mandal, P., Chaudhuri, S., et al. (2020). Suppression of poised oncogenes by ZMYND8 promotes chemo-sensitization. Cell Death Dis. *11*, 1073–1118. https://doi.org/10.1038/s41419-020-03129-x.

38. Saha, S., Mukherjee, S., Khan, P., Kajal, K., Mazumdar, M., Manna, A., Mukherjee, S., De, S., Jana, D., Sarkar, D.K., and Das, T. (2016). Aspirin Suppresses the Acquisition of Chemoresistance in Breast Cancer by Disrupting an NFκB–IL6 Signaling Axis Responsible for the Generation of Cancer Stem Cells. Cancer Res. *76*, 2000–2012. https://doi.org/10.1158/0008-5472.CAN-15-1360.

39. R2: Open Online Genomics Analysis & Visualization Platform. https://hgserver1.amc.nl/cgi-bin/r2/main.cgi?open_page=login.

40. Lánczky, A., and Győrffy, B. (2021). Web-Based Survival Analysis Tool Tailored for Medical Research (KMplot): Development and Implementation. J. Med. Internet Res. *23*, e27633. https://doi.org/10.2196/27633.

41. Dreos, R., Ambrosini, G., Périer, R.C., and Bucher, P. (2015). The Eukaryotic Promoter Database: expansion of EPDnew and new promoter analysis tools. Nucleic Acids Res. *43*, D92–D96. https://doi.org/10.1093/nar/gku1111.

42. Meylan, P., Dreos, R., Ambrosini, G., Groux, R., and Bucher, P. (2020). EPD in 2020: enhanced data visualization and extension to ncRNA promoters. Nucleic Acids Res. *48*, D65–D69. https://doi.org/10.1093/nar/gkz1014.

43. Castro-Mondragon, J.A., Riudavets-Puig, R., Rauluseviciute, I., Lemma, R.B., Turchi, L., Blanc-Mathieu, R., Lucas, J., Boddie, P., Khan, A., Manosalva Pérez, N., et al. (2022). JASPAR 2022: the 9th release of the open-access database of transcription factor binding profiles. Nucleic Acids Res. *50*, D165–D173. https://doi.org/10.1093/nar/gkab1113.

44. Saleem, R.A., Banerjee-Basu, S., Murphy, T.C., Baxevanis, A., and Walter, M.A. (2004). Essential structural and functional determinants within the forkhead domain of FOXC1. Nucleic Acids Res. *32*, 4182–4193. https://doi.org/10.1093/nar/gkh742.

45. Zheng, X., Cui, D., Xu, S., Brabant, G., and Derwahl, M. (2010). Doxorubicin fails to eradicate cancer stem cells derived from anaplastic thyroid carcinoma cells: Characterization of resistant cells. Int. J. Oncol. *37*, 307–315. https://doi.org/10.3892/ijo_00000679.

46. Nedeljković, M., and Damjanović, A. (2019). Mechanisms of Chemotherapy Resistance in Triple-Negative Breast Cancer—How We Can Rise to the Challenge. Cells *8*, 957. https://doi.org/10.3390/cells8090957.

47. Backes, C., Fehlmann, T., Kern, F., Kehl, T., Lenhof, H.-P., Meese, E., and Keller, A. (2018). miRCarta: a central repository for collecting miRNA candidates. Nucleic Acids Res. *46*, D160–D167. https://doi.org/10.1093/nar/gkx851.

48. Paraskevopoulou, M.D., Georgakilas, G., Kostoulas, N., Vlachos, I.S., Vergoulis, T., Reczko, M., Filippidis, C., Dalamagas, T., and Hatzigeorgiou, A.G. (2013). DIANA-microT web server v5.0: service integration into miRNA functional analysis workflows. Nucleic Acids Res. *41*, W169–W173. https://doi.org/10.1093/nar/gkt393.

49. Zhao, M., Chang, J., Liu, R., Liu, Y., Qi, J., Wang, Y., Zhang, X., Qiao, L., Jin, Y., An, H., and Ren, L. (2020). miR-495 and miR-5688 are down-regulated in non-small cell lung cancer under hypoxia to maintain interleukin-11 expression. Cancer Commun. *40*, 435–452. https://doi.org/10.1002/cac2.12076.

50. Prabhakaran, P., Hassiotou, F., Blancafort, P., and Filgueira, L. (2013). Cisplatin induces differentiation of breast cancer cells. Front. Oncol. *3*, 134. https://doi.org/10.3389/fonc.2013.00134.

51. Bussolati, B., Grange, C., Sapino, A., and Camussi, G. (2009). Endothelial cell differentiation of human breast tumour stem/progenitor cells. J. Cell Mol. Med. *13*, 309–319. https://doi.org/10.1111/j.1582-4934.2008.00338.x.

52. Liao, X.-H., Wang, Y., Wang, N., Yan, T.-B., Xing, W.-J., Zheng, L., Zhao, D.-W., Li, Y.-Q., Liu, L.-Y., Sun, X.-G., et al. (2014). Human chorionic gonadotropin decreases human breast cancer cell proliferation and promotes differentiation. IUBMB Life *66*, 352–360. https://doi.org/10.1002/iub.1269.

53. Bhattacharya, A., Mukherjee, S., Khan, P., Banerjee, S., Dutta, A., Banerjee, N., Sengupta, D., Basak, U., Chakraborty, S., Dutta, A., et al. (2020). SMAR1 repression by pluripotency factors and consequent chemoresistance in breast cancer stem-like cells is reversed by aspirin. Sci. Signal. *13*, eaay6077. https://doi.org/10.1126/scisignal.aay6077.

54. Konieczkowski, D.J., Johannessen, C.M., and Garraway, L.A. (2018). A convergence-based framework for cancer drug resistance. Cancer Cell *33*, 801–815. https://doi.org/10.1016/j.ccell.2018.03.025.

55. Nairuz, T., Mahmud, Z., Manik, R.K., and Kabir, Y. (2023). Cancer stem cells: an insight into the development of metastatic tumors and therapy resistance. Stem Cell Rev. Rep. *19*, 1577–1595. https://doi.org/10.1007/s12015-023-10529-x.

56. Longacre, M., Snyder, N.A., Housman, G., Leary, M., Lapinska, K., Heerboth, S., Willbanks, A., and Sarkar, S. (2016). A Comparative Analysis of Genetic and Epigenetic Events of Breast and Ovarian Cancer Related to Tumorigenesis. Int. J. Mol. Sci. *17*, 759. https://doi.org/10.3390/ijms17050759.

57. Heerboth, S., Lapinska, K., Snyder, N., Leary, M., Rollinson, S., and Sarkar, S. (2014). Use of Epigenetic Drugs in Disease: An Overview. Genet. Epigenet. *6*, 9–19. https://doi.org/10.4137/GEG.S12270.

58. Sarkar, S., Horn, G., Moulton, K., Oza, A., Byler, S., Kokolus, S., and Longacre, M. (2013). Cancer Development, Progression, and Therapy: An Epigenetic Overview. Int. J. Mol. Sci. *14*, 21087–21113. https://doi.org/10.3390/ijms141021087.

59. Heerboth, S., Housman, G., Leary, M., Longacre, M., Byler, S., Lapinska, K., Willbanks, A., and Sarkar, S. (2015). EMT and tumor metastasis. Clin. Transl. Med. *4*, 6. https://doi.org/10.1186/s40169-015-0048-3.

60. Sarkar, S., Goldgar, S., Byler, S., Rosenthal, S., and Heerboth, S. (2013). Demethylation and re-expression of epigenetically silenced tumor suppressor genes: sensitization of cancer cells by combination therapy. Epigenomics *5*, 87–94. https://doi.org/10.2217/epi.12.68.

61. Byler, S., Goldgar, S., Heerboth, S., Leary, M., Housman, G., Moulton, K., and Sarkar, S. (2014). Genetic and epigenetic aspects of breast cancer progression and therapy. Anticancer Res. *34*, 1071–1077.

62. Xu, Y.L., Yao, R., Li, J., Zhou, Y.D., Mao, F., Pan, B., and Sun, Q. (2017). FOXC1 overexpression is a marker of poor response to anthracycline-based adjuvant chemotherapy in sporadic triple-negative breast cancer. Cancer Chemother. Pharmacol. *79*, 1205–1213. https://doi.org/10.1007/s00280-017-3319-4.

63. Kumar, U., Hu, Y., Masrour, N., Castellanos-Uribe, M., Harrod, A., May, S.T., Ali, S., Speirs, V., Coombes, R.C., and Yagüe, E. (2021). MicroRNA-495/TGF-β/FOXC1 axis regulates multidrug resistance in metaplastic breast cancer cells. Biochem. Pharmacol. *192*, 114692. https://doi.org/10.1016/j.bcp.2021.114692.

64. Lu, Y.-T., Xu, T., Iqbal, M., Hsieh, T.-C., Luo, Z., Liang, G., Farnham, P.J., Rhie, S.K., and Goldkorn, A. (2022). FOXC1 Binds Enhancers and Promotes Cisplatin Resistance in Bladder Cancer. Cancers (Basel) *14*, 1717. https://doi.org/10.3390/cancers14071717.

65. Mohiuddin, I.S., Wei, S.-J., and Kang, M.H. (2020). Role of OCT4 in cancer stem-like cells and chemotherapy resistance. Biochim. Biophys. Acta, Mol. Basis Dis. *1866*, 165432. https://doi.org/10.1016/j.bbadis.2019.03.005.

66. Lee, S.H., Oh, S.-Y., Do, S.I., Lee, H.J., Kang, H.J., Rho, Y.S., Bae, W.J., and Lim, Y.C. (2014). SOX2 regulates self-renewal and tumorigenicity of stem-like cells of head and neck squamous cell carcinoma. Br. J. Cancer *111*, 2122–2130. https://doi.org/10.1038/bjc.2014.528.

67. Zhang, J., Espinoza, L.A., Kinders, R.J., Lawrence, S.M., Pfister, T.D., Zhou, M., Veenstra, T.D., Thorgeirsson, S.S., and Jessup, J.M. (2013). NANOG modulates

stemness in human colorectal cancer. Oncogene *32*, 4397–4405. https://doi.org/10.1038/onc.2012.461.

68. Mukherjee, S., Manna, A., Bhattacharjee, P., Mazumdar, M., Saha, S., Chakraborty, S., Guha, D., Adhikary, A., Jana, D., Gorain, M., et al. (2016). Non-migratory tumorigenic intrinsic cancer stem cells ensure breast cancer metastasis by generation of CXCR4(+) migrating cancer stem cells. Oncogene *35*, 4937–4948. https://doi.org/10.1038/onc.2016.26.

69. Iwamoto, T., Kajiwara, Y., Zhu, Y., and Iha, S. (2020). Biomarkers of neoadjuvant/adjuvant chemotherapy for breast cancer. Chin. Clin. Oncol. *9*, 27. https://doi.org/10.21037/cco.2020.01.06.

70. Riedinger, C.J., Kimball, K.J., Kilgore, L.C., Bell, C.W., Heidel, R.E., and Boone, J.D. (2020). Water only fasting and its effect on chemotherapy administration in gynecologic malignancies. Gynecol. Oncol. *159*, 799–803. https://doi.org/10.1016/j.ygyno.2020.09.008.

71. Meng, T., Liu, J., Wen, L., Yuan, M., Cheng, B., Hu, Y., Zhu, Y., Liu, X., Yuan, H., and Hu, F. (2016). Multi-cycle chemotherapy with the glycolipid-like polymeric micelles evade cancer stem cell enrichment in breast cancer therapy. Oncotarget *7*, 72978–72989. https://doi.org/10.18632/oncotarget.12159.

72. Kahraman, M., Röske, A., Laufer, T., Fehlmann, T., Backes, C., Kern, F., Kohlhaas, J., Schrörs, H., Saiz, A., Zabler, C., et al. (2018). MicroRNA in diagnosis and therapy monitoring of early-stage triple-negative breast cancer. Sci. Rep. *8*, 11584. https://doi.org/10.1038/s41598-018-29917-2.

73. Liu, H. (2012). MicroRNAs in breast cancer initiation and progression. Cell. Mol. Life Sci. *69*, 3587–3599. https://doi.org/10.1007/s00018-012-1128-9.

74. Mukherjee, S., Mazumdar, M., Chakraborty, S., Manna, A., Saha, S., Khan, P., Bhattacharjee, P., Guha, D., Adhikary, A., Mukhjerjee, S., and Das, T. (2014). Curcumin inhibits breast cancer stem cell migration by amplifying the E-cadherin/β-catenin negative feedback loop. Stem Cell Res. Ther. *5*, 116. https://doi.org/10.1186/scrt506.

75. Sarkar, T., Dhar, S., Chakraborty, D., Pati, S., Bose, S., Panda, A.K., Basak, U., Chakraborty, S., Mukherjee, S., Guin, A., et al. (2022). FOXP3/HAT1 Axis Controls Treg Infiltration in the Tumor Microenvironment by Inducing CCR4 Expression in Breast Cancer. Front. Immunol. *13*, 740588. https://doi.org/10.3389/fimmu.2022.740588.

76. Meister, G., Landthaler, M., Dorsett, Y., and Tuschl, T. (2004). Sequence-specific inhibition of microRNA- and siRNA-induced RNA silencing. RNA *10*, 544–550. https://doi.org/10.1261/rna.5235104.

77. Doherty, M.R., Smigiel, J.M., Junk, D.J., and Jackson, M.W. (2016). Cancer Stem Cell Plasticity Drives Therapeutic Resistance. Cancers *8*, 8. https://doi.org/10.3390/cancers8010008.

78. Mukherjee, S., Chakraborty, S., Basak, U., Pati, S., Dutta, A., Dutta, S., Roy, D., Banerjee, S., Ray, A., Sa, G., and Das, T. (2023). Breast cancer stem cells generate immune-suppressive T regulatory cells by secreting TGFβ to evade immune-elimination. Discov. Oncol. *14*, 220. https://doi.org/10.1007/s12672-023-00787-z.

79. L, D.W. (2002). The PyMOL Molecular Graphics System (De-Lano Scientific). http://www.pymol.org.

80. Li, S., Olson, W.K., and Lu, X.-J. (2019). Web 3DNA 2.0 for the analysis, visualization, and modeling of 3D nucleic acid structures. Nucleic Acids Res. *47*, W26–W34. https://doi.org/10.1093/nar/gkz394.

81. de Vries, S.J., van Dijk, M., and Bonvin, A.M.J.J. (2010). The HADDOCK web server for data-driven biomolecular docking. Nat. Protoc. *5*, 883–897. https://doi.org/10.1038/nprot.2010.32.

82. Michael, A.K., Grand, R.S., Isbel, L., Cavadini, S., Kozicka, Z., Kempf, G., Bunker, R. D., Schenk, A.D., Graff-Meyer, A., Pathare, G.R., et al. (2020). Mechanisms of OCT4-SOX2 motif readout on nucleosomes. Science *368*, 1460–1465. https://doi.org/10.1126/science.abb0074.

83. Holmes, Z.E., Hamilton, D.J., Hwang, T., Parsonnet, N.V., Rinn, J.L., Wuttke, D.S., and Batey, R.T. (2020). The Sox2 transcription factor binds RNA. Nat. Commun. *11*, 1805. https://doi.org/10.1038/s41467-020-15571-8.